


Photon-photon interactions in dynamically coupled cavities

Mikkel Heuck ^{1,2,*}, Kurt Jacobs,^{3,4,5} and Dirk R. Englund²

¹*DTU Fotonik, Technical University of Denmark, Building 343, 2800 Kongens Lyngby, Denmark*

²*Department of Electrical Engineering and Computer Science, Massachusetts Institute of Technology, 77 Massachusetts Avenue, Cambridge, Massachusetts 02139, USA*

³*U.S. Army Research Laboratory, Computational and Information Sciences Directorate, Adelphi, Maryland 20783, USA*

⁴*Department of Physics, University of Massachusetts at Boston, Boston, Massachusetts 02125, USA*

⁵*Hearne Institute for Theoretical Physics, Louisiana State University, Baton Rouge, Louisiana 70803, USA*



(Received 1 October 2019; accepted 16 March 2020; published 20 April 2020)

We study theoretically the interaction between two photons in a nonlinear cavity. The photons are absorbed into the cavity by an effective tuning of its input-output coupling via external control of a coupling to a second, strongly output-coupled cavity mode. Such “dynamically coupled” cavities, which can be implemented using bulk $\chi^{(2)}$ and $\chi^{(3)}$ nonlinearities, enable incoming photon wave packets to be absorbed into the cavity with high fidelity when the duration of the control is similar to that of the wave packets. Further, this configuration can be used to avoid limitations in the photon-photon interaction time set by the delay-bandwidth product of passive cavities and enables the elimination of wave-packet distortions caused by dispersive cavity transmission and reflection. We consider three kinds of nonlinearities, two arising from $\chi^{(2)}$ and $\chi^{(3)}$ materials and one due to an interaction with a two-level emitter. To analyze the input and output of few-photon wave packets, we use a Schrödinger-picture formalism in which traveling-wave fields are discretized into infinitesimal time bins. We suggest that dynamically coupled cavities provide a very useful tool for improving the performance of quantum devices relying on cavity-enhanced light-matter interactions such as single-photon sources and atomlike quantum memories with photon interfaces. As an example, we present simulation results showing that high-fidelity two-qubit entangling gates may be constructed using any of the considered nonlinear interactions.

DOI: [10.1103/PhysRevA.101.042322](https://doi.org/10.1103/PhysRevA.101.042322)

I. INTRODUCTION

Photons make excellent flying qubits due to the low decoherence and loss associated with their transport over standard telecommunication fibers. It therefore seems unavoidable that they will play a key role as carriers of quantum information for secure communication networks and distributed quantum computing [1]. The lack of direct interactions between photons makes it very challenging to perform universal quantum information processing using photonic qubits. Indirect interactions may be mediated by materials with optical nonlinearities but these are usually very weak at optical frequencies. Nevertheless, progress in the design and fabrication of nanocavities with very small mode volumes and very large lifetimes [2–6] has reduced the optical energy required to observe nonlinear interactions close to the single-photon level. To fully exploit the enhanced light-matter interaction inside the cavity, it is necessary for the entire energy of an incoming wave packet to reside in the cavity throughout its lifetime. However, delay-bandwidth trade-offs [7] put bounds on the energy from an incoming wave packet that can reside inside a passive cavity throughout its lifetime. For instance, a rising exponential wave packet may be absorbed completely into a cavity, but only for an infinitesimal time, such that the average energy is smaller than the total incoming energy. The

delay-bandwidth limit may be broken using active controls to modify the cavity-waveguide coupling at a timescale smaller than the wave-packet temporal width. Such dynamically coupled cavities have been demonstrated in photonic crystals [8] and ring resonators [9]. These demonstrations used short optical pump pulses to generate electric charge carriers in the semiconductor material forming the cavities. The free carrier absorption loss associated with this method degrades the intrinsic quality factor, Q_L , which motivates the search for an alternative approach.

Here, we use a method to achieve dynamic coupling that is based on the parametric nonlinearity of cavity materials ($\chi^{(2)}$ or $\chi^{(3)}$) and therefore avoids loss. Two strong optical control fields may couple two cavity modes via so-called Bragg-scattering four-wave mixing (FWM) in $\chi^{(3)}$ materials [10–12] and a single control field may do the same in a $\chi^{(2)}$ material [5,13], as illustrated with arrows in Fig. 1(b). Matching the path-length imbalance of the Mach-Zehnder interferometer coupling region [see Fig. 1(a)] to the round-trip length of the ring causes destructive interference at ω_b (no coupling) and constructive interference at ω_a (maximal coupling); see Fig. 1(b). External control over the coupling between modes a and b therefore introduces a time-dependent effective coupling between mode b and the waveguide [12,14]. In other words, photons may be loaded in and out of mode b via the strongly coupled mode, a , due to their time-dependent mutual coupling. We note that this method has also been proposed to implement so-called quantum pulse gates [15].

*mheuck@mit.edu

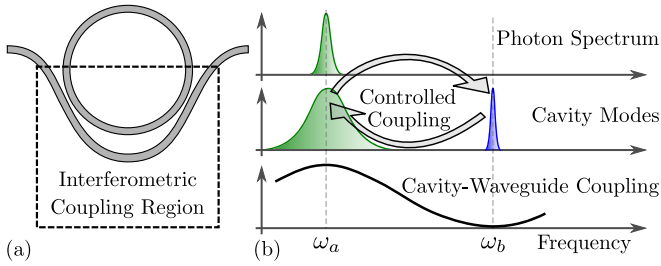


FIG. 1. (a) Ring resonator with a Mach-Zehnder interferometer coupling region for frequency-dependent cavity-waveguide coupling rate. (b) Spectra of the incoming photon wave packet (top), cavity modes a (oscillating at ω_a) and b (oscillating at ω_b) coupled via external control fields (center), and cavity-waveguide coupling rate (bottom).

We succinctly review a Schrödinger picture, discrete-time formalism for treating input and output from optical cavities (equivalent to the well-known Heisenberg-picture input-output formalism [16–18]), and show how it can be used to treat the input-output of one- and two-photon wave packets into and out of dynamically coupled nonlinear cavities. We suggest that dynamically coupled cavities would be useful for a range of quantum applications relying on cavity-enhanced light-matter interaction, and specifically use the formalism to calculate the fidelity of two-qubit gates for traveling-wave photons.

The method we develop here for treating the effect of localized systems on few-photon wave packets is not the first. The basic formalism for this scattering problem for Markovian systems is input-output theory [16,17]. While scattering of one or two photons from sufficiently simple systems can be solved analytically [19–29], previous numerical methods can be divided into two types. The most direct is essentially a brute-force approach in which the field is discretized and the full state of the system and field is simulated [30–32]. The second method, derived from input-output theory for general systems by Caneva *et al.* [33] and Trivadi *et al.* [34], involves calculating the “scattering matrix” (or Green’s function-impulse response) that maps δ -function input wave packets to output wave packets. For an N -photon wave packet, the scattering “matrix” is a function of $2N$ variables, and for a given input the output is calculated by integrating it over the input wave packet. This method is more numerically efficient than the brute-force method because the scattering matrix can be determined by solving the equations of motion of the system alone [33,34]. The method we present here is somewhat more efficient numerically than the above method. We derive equations of motion that are driven by the input wave packet(s), and the solutions of these for a set of shifted times gives the output wave packet(s). This requires a similar amount of numerical overhead as the calculation of the scattering matrix, and thus avoids the final step of integrating the scattering matrix over the input wave packet(s) to determine the output. Our equations are derived from a Schrödinger-picture version of input-output theory and correspond to a diagram that describes the various “pathways” that photons can take by being absorbed and emitted from the system. They thus provide a more detailed understanding of the dynamics

of the scattering process than previous methods. The disadvantage of our method is that more work is required to derive the equations of motion than for the scattering method. We also note that if one wishes to calculate the output for a large number of different inputs, there will be a point at which it will be more efficient to calculate the scattering matrix. Finally, we note that Baragiola *et al.* [35] have derived master equations describing the evolution of Markovian systems driven by N -photon wave packets, although they did not provide a method to obtain the output wave packets.

This article is organized as follows: Section II describes the discrete-time formalism and Sec. III elucidates the Hamiltonians that describe our nonlinear cavity modes. In Sec. IV, we consider the linear regime and examine the dynamics of the cavity modes under the controlled coupling. In Sec. V we present analytic solutions for the control fields required to absorb and emit wave packets with predefined shapes and consider a specific example in which the wave packets are Gaussian. Section VI contains a description of three types of nonlinear interactions, $\chi^{(2)}$, $\chi^{(3)}$, and two-level emitters (TLEs), and considers their application to controlled-phase (C-phase) gates. Finally, we conclude with a discussion of the limitations of our model and suggest other quantum applications that could benefit from dynamically coupled cavities.

II. DISCRETE-TIME FORMALISM

In our analysis of the dynamics of photons scattering off a system driven by external control fields, we discretize the traveling-wave field into time bins of duration Δt as illustrated in Fig. 2 [36–38]. The time axis may be thought of as a conveyor belt and time evolution corresponds to dragging this conveyor belt past the fixed system one bin at a time. The discretization involves introducing new field operators

$$\hat{w}(t_k) = \hat{w}(k\Delta t) \equiv \frac{\hat{w}_k}{\sqrt{\Delta t}} \quad \text{with} \quad [\hat{w}_j, \hat{w}_k^\dagger] = \delta_{jk}, \quad (1)$$

where $\hat{w}(t_k)$ is the continuous-time annihilation operator that removes a photon from the waveguide at time $t_k = k\Delta t$. The operator \hat{w}_k is the discrete-time counterpart of $\hat{w}(t_k)$ that removes a photon from the k th time bin. The factor of $1/\sqrt{\Delta t}$

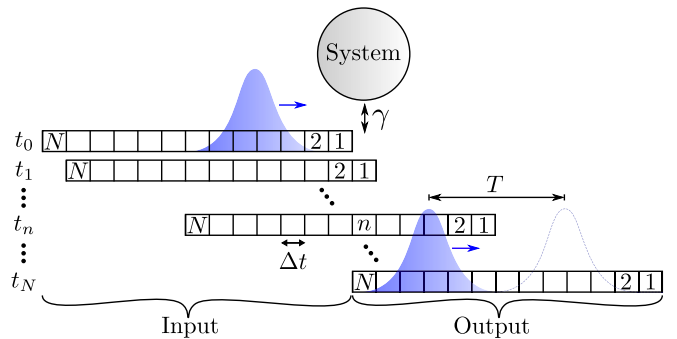


FIG. 2. Illustration of the discrete time formalism. The time axis for the traveling-wave field is divided into discrete bins and time evolution is modeled by shifting the time axis from left to right. The system interacts with one time bin at a time, modeling a point-interaction with the field as is standard in the input-output formalism for quantum systems.

allows $\hat{w}(t_k)$ to have the canonical commutation relation, $[\hat{w}(t_j), \hat{w}^\dagger(t_k)] = \delta(t_j - t_k)$, as $\Delta t \rightarrow 0$.

For a single-photon input with a wave packet described by $\xi_{\text{in}}(t)$, the continuous and discrete descriptions are

$$|\psi_{\text{in}}\rangle = \int_{t_0}^{t_N} dt \xi_{\text{in}}(t) \hat{w}^\dagger(t) |\emptyset\rangle \approx \sum_{k=1}^N \sqrt{\Delta t} \xi_k^{\text{in}} \hat{w}_k^\dagger |\emptyset\rangle, \quad (2)$$

in which $\int_{t_0}^{t_N} |\xi_{\text{in}}(t)|^2 dt = 1$ so the state is normalized, $\xi_k^{\text{in}} = \xi_{\text{in}}(t_k)$, and $|\emptyset\rangle$ denotes the vacuum state of the waveguide. At any time step, n (see Fig. 2), a photon in bin k , is referred to as an *input* photon if $k > n$ and we write the corresponding state of the field as $\hat{w}_k^\dagger |\emptyset\rangle \equiv |1_k\rangle$. Similarly, if $k \leq n$, the photon is referred to as an *output* photon and we denote the corresponding state of the field by $|1_k\rangle$. A system consisting of M cavity modes is described by a state $|\psi_{\text{sys}}\rangle = \psi_{n_a n_b \dots n_M}(t) |n_a\rangle |n_b\rangle \dots |n_M\rangle$, where, e.g., n_a is the number of photons in mode a (oscillating at ω_a); see Fig. 1.

We use the Schrödinger picture to derive equations of motion for the time-dependent state coefficients. The unitary time evolution operator describing one time step from t_{n-1} to t_n in Fig. 2 is

$$\hat{U}_n = \exp\left(-\frac{i}{\hbar} \hat{H}_n \Delta t\right) = \sum_{m=0}^{\infty} \frac{1}{m!} \left(-\frac{i}{\hbar} \hat{H}_n \Delta t\right)^m, \quad (3)$$

such that the updated state is

$$|\psi_n\rangle = \hat{U}_n |\psi_{n-1}\rangle, \quad (4)$$

with \hat{H}_n being the Hamiltonian describing the system and its interaction with the waveguide at time step n . In the next section, we explain the model used to describe the system and its interaction with the waveguide and additional loss channels.

III. MODEL

A model for the complete system consists of a specification of the Hamiltonian in Eq. (3). It is assumed that the interaction between the system and waveguide occurs at a singular spatial point, which corresponds to interaction only with bin n at time t_n . It is therefore convenient to think of N different Hamiltonians, \hat{H}_n , each acting only during the n th time step.

In our analysis, the system in Fig. 2 contains up to three cavity modes and one TLE. Only mode a is coupled to the waveguide in order to load and unload photons into and out of mode b (oscillating at ω_b); see Fig. 1. Our choice of cavity mode configurations is motivated by the type of photon-photon interaction and application (C-phase gate) that we are considering. For a $\chi^{(3)}$ nonlinearity, we consider the photon-number-dependent phase acquired by the field in mode b through self-phase modulation. For a $\chi^{(2)}$ nonlinearity, we consider an additional mode, c (oscillating at $\omega_c = 2\omega_b$), which is coupled to mode b through second harmonic generation (SHG). Two photons loaded into mode b acquire a π -phase shift by undergoing one Rabi oscillation (turning into one photon in mode c and back to two photons in mode b). A single photon in mode b does not acquire any phase because SHG requires at least two photons. For a TLE, we again consider a third mode (oscillating at ω_c with $|\omega_c - \omega_b| \neq$

$|\omega_b - \omega_a|$), which is coupled to the TLE. In this case, the acquired phase of the field in mode c is photon number dependent since the resonance experiences an energy-shift proportional to \sqrt{ng} for n photons and a TLE-cavity coupling rate, g .

The self-energy terms of the system Hamiltonian in a rotating frame (also known as the interaction picture; see Appendix A) are

$$\hat{H}_0 = \hbar \delta_a \hat{a}^\dagger \hat{a} + \hbar \delta_b \hat{b}^\dagger \hat{b} + \hbar \delta_c \hat{c}^\dagger \hat{c} + \hbar \delta_e \hat{\sigma}_z, \quad (5)$$

where \hat{a} , \hat{b} , and \hat{c} annihilate a photon from modes a , b , and c . The operator $\hat{\sigma}_z = |e\rangle\langle e|$, with $|e\rangle$ being the excited state of a TLE coupled to mode c . The detunings, δ_n , are used to account for discrepancies between energy levels of the system and the incoming photons and control fields as described in Appendix A.

Coupling between the waveguide and mode a is described by the Hamiltonian [37]

$$\hat{H}_n^{\text{cav-wg}} = i\hbar \sqrt{\frac{\gamma}{\Delta t}} (\hat{a}^\dagger \hat{w}_n - \hat{a} \hat{w}_n^\dagger), \quad (6)$$

where γ is the coupling rate.

As mentioned above, a dynamic cavity-waveguide coupling is established by coupling two cavity modes, one strongly coupled and one decoupled from the waveguide, via nonlinear interactions driven by external control fields. In materials with a third-order nonlinearity, $\chi^{(3)}$, the coupling Hamiltonian is

$$\hat{H}_n^{\text{cav-cav}} = \hbar \chi_3 (\hat{\rho}_1^\dagger \hat{\rho}_2 \hat{a}^\dagger \hat{b} + \hat{\rho}_2^\dagger \hat{\rho}_1 \hat{b}^\dagger \hat{a}), \quad (7)$$

The operators $\hat{\rho}_1$ and $\hat{\rho}_2$ annihilate photons from two pump modes far detuned from modes a , b , and c . The pump fields are treated classically by taking expectation values and making the substitution [39]

$$\chi_3 \langle \hat{\rho}_2^\dagger \hat{\rho}_1 \rangle = \chi_3 \alpha_2^*(t_n) \alpha_1(t_n) \equiv \Lambda(t_n), \quad (8)$$

where α_n is the eigenvalue of the annihilation operator $\hat{\rho}_n$ and $\Lambda(t_n)$ is the complex-valued control field. With the classical control field, Eq. (7) reads

$$\hat{H}_n^{\text{cav-cav}} = \hbar (\Lambda_n^* \hat{a}^\dagger \hat{b} + \Lambda_n \hat{b}^\dagger \hat{a}), \quad (9)$$

which now describes a linear coupling between modes a and b driven by the time-dependent control field, $\Lambda(t)$. Note that in the case of a TLE nonlinearity, we introduce a second control field, $\Pi(t)$, that couples modes b and c using pump modes p_1 and another mode p_3 ; see Appendix A.

For $\chi^{(3)}$ materials, we must also include the cross-phase modulation caused by the pump fields on modes a , b , and c described by the Hamiltonian

$$\begin{aligned} \hat{H}_n^{\text{XPM,P}} &= \hbar \chi_3 \sum_{m=1}^2 \hat{\rho}_m^\dagger \hat{\rho}_m (\hat{a}^\dagger \hat{a} + \hat{b}^\dagger \hat{b} + \hat{c}^\dagger \hat{c}) \\ &\rightarrow 2\hbar |\Lambda_n| (\hat{a}^\dagger \hat{a} + \hat{b}^\dagger \hat{b} + \hat{c}^\dagger \hat{c}), \end{aligned} \quad (10)$$

where we have assumed $\chi_3 \langle \hat{\rho}_2^\dagger \hat{\rho}_2 \rangle = \chi_3 \langle \hat{\rho}_1^\dagger \hat{\rho}_1 \rangle = |\Lambda_n|$, which means that the optical energy in each pump mode is identical at all times.

In a $\chi^{(2)}$ material, the cavity-cavity coupling arises from the Hamiltonian

$$\hat{H}_n^{\text{cav-cav}} = \hbar \chi_2 (\hat{\rho}^\dagger \hat{a}^\dagger \hat{b} + \hat{\rho} \hat{b}^\dagger \hat{a}). \quad (11)$$

Again, we describe it classically by

$$\chi_2(\hat{p}) = \chi_2 \alpha_p(t_n) \equiv \Lambda_n. \quad (12)$$

The coupling Hamiltonian expressed in terms of the classical control field is therefore given by Eq. (9) for both second- and third-order nonlinear materials. There is no cross-phase modulation term in the Hamiltonian for a $\chi^{(2)}$ material (unless a DC electric field is applied), so the contribution from Eq. (10) should be omitted in that case.

The Hamiltonian describing the three different types of nonlinear materials are

$$\begin{aligned} \hat{H}_{\text{XPM}} + \hat{H}_{\text{SPM}} &= \hbar \chi_3 [\hat{a}^\dagger \hat{a} \hat{b}^\dagger \hat{b} + \hat{b}^\dagger \hat{b} \hat{c}^\dagger \hat{c}] \\ &+ \frac{\hbar \chi_3}{4} \sum_{\hat{q}} (\hat{q}^\dagger \hat{q} - 1) \hat{q}^\dagger \hat{q}, \end{aligned} \quad (13a)$$

$$\hat{H}_{\text{SHG}} = \hbar \chi_2 (\hat{c} \hat{b}^\dagger \hat{b}^\dagger + \hat{c}^\dagger \hat{b} \hat{b}), \quad (13b)$$

$$\hat{H}_{\text{TLE}} = \hbar (g \hat{c}^\dagger \hat{\sigma}_- + g^* \hat{c} \hat{\sigma}_+). \quad (13c)$$

Equation (13a) describes cross- (XPM) and self-phase modulation (SPM) in materials with a third-order nonlinearity (note that $\hat{q} \in \{\hat{a}, \hat{b}, \hat{c}\}$). Equation (13b) describes second harmonic generation (SHG) in materials with second-order nonlinearities. Equation (13c) describes the interaction between photons in mode c and a two-level emitter, where g is the coupling rate, $\hat{\sigma}_- \equiv |g\rangle\langle e|$, and $\hat{\sigma}_+ \equiv |e\rangle\langle g|$, where $|g\rangle$ and $|e\rangle$ are the ground and excited states of the TLE. Note that not all possible combinations of modes are considered in (13), but only those included in the protocols for photon-photon interactions that we consider here.

IV. LINEAR DYNAMICS

In this section, we derive equations of motion including only the linear dynamics. We start with the simplest case of one photon coupling to one cavity mode to build intuition about the derivation procedure. Then, we consider one photon coupling to a cavity with two modes, and finally two photons coupling to a cavity with two modes. Having derived equations of motion when the Hamiltonian is linear, it is fairly straightforward to add nonlinear interactions and make the appropriate additions to the equations, which we do in Sec. VI.

A. One cavity mode and one photon

Let us begin by considering a single input photon coupling to one cavity mode. The relevant terms of the Hamiltonian are

$$\hat{H}_n^{(1)} = \hbar \delta_a \hat{a}^\dagger \hat{a} + i \hbar \sqrt{\frac{\gamma}{\Delta t}} (\hat{a}^\dagger \hat{w}_n - \hat{a} \hat{w}_n^\dagger). \quad (14)$$

Keeping only terms to first order in Δt , the corresponding time-evolution operator is

$$\begin{aligned} \hat{U}_n^{(1)} &\approx \hat{\mathbb{1}} + \sqrt{\gamma \Delta t} (\hat{a}^\dagger \hat{w}_n - \hat{a} \hat{w}_n^\dagger) - \frac{\gamma}{2} \Delta t \hat{a}^\dagger \hat{a} \hat{w}_n \hat{w}_n^\dagger \\ &- i \delta_a \Delta t \hat{a}^\dagger \hat{a}. \end{aligned} \quad (15)$$

Note that we omitted the term $\gamma/2 \Delta t \hat{a} \hat{a}^\dagger \hat{w}_n^\dagger \hat{w}_n$ because it results in terms proportional to $\Delta t^{3/2}$ when acting on states

with the photon in the waveguide. The state at time step n is

$$\begin{aligned} |\psi_n\rangle &= \sum_{k=n+1}^N \xi_k^{\text{in}} \sqrt{\Delta t} |0\rangle |1_k\rangle + \sum_{k=1}^n \xi_k^{\text{out}} \sqrt{\Delta t} |0\rangle |1_k\rangle \\ &+ \psi_1(n) |1\rangle |\emptyset\rangle. \end{aligned} \quad (16)$$

The states $|0\rangle |1_k\rangle$ and $|0\rangle |\mathbf{1}_k\rangle$ correspond to an empty cavity and a photon in bin k on the input ($k > n$) and output ($k \leq n$) sides, respectively. The state corresponding to a photon in the cavity has the coefficient $\psi_1(n)$. In Appendix B, we derive the equation of motion for $\psi_1(t)$ and the input-output relation connecting $\xi_{\text{out}}(t)$ to $\xi_{\text{in}}(t)$

$$\dot{\psi}_1(t) = -\left(i\delta_a + \frac{\gamma}{2}\right) \psi_1(t) + \sqrt{\gamma} \xi_{\text{in}}(t), \quad (17a)$$

$$\xi_{\text{out}}(t) = \xi_{\text{in}}(t) - \sqrt{\gamma} \psi_1(t). \quad (17b)$$

These equations have the same form as those derived classically using arguments of energy conservation and time-reversal symmetry [40]. They also have the same form as the Heisenberg equations of motion of the usual input-output formalism [41].

B. Loss

At this stage we consider the effect of loss through coupling of the system to a heat bath at zero temperature. It may be conveniently modeled using an additional waveguide with a vacuum input. If the annihilation operator that removes a photon from the bath at time t_n is \hat{l}_n , then the time-evolution operator has the additional terms

$$\hat{U}_n^{\text{loss}} = \sum_{\hat{q}} [\sqrt{\gamma_L \Delta t} (\hat{q}^\dagger \hat{l}_n - \hat{q} \hat{l}_n^\dagger) - \frac{\gamma_L}{2} \Delta t \hat{q}^\dagger \hat{q} \hat{l}_n \hat{l}_n^\dagger], \quad (18)$$

where \hat{q} represents all the cavity modes (we assume they have identical loss rates, γ_L). If we ignore all states of the loss channel except the vacuum, Eq. (18) shows that a term, $-\gamma_L/2$, is added to all decay terms (with n photons in the cavity mode), such that the decay term in Eq. (17a) would have the coefficient $-(\gamma + \gamma_L)/2$. We therefore define the total coupling rate, $\Gamma = \gamma + \gamma_L$. If we kept track of the state of the heat bath, \mathcal{B} , the complete state after time evolution is

$$|\Theta\rangle = |\theta_0\rangle |0_{\mathcal{B}}\rangle + |\theta_1\rangle |1_{\mathcal{B}}\rangle + \dots + |\theta_{\mathcal{N}}\rangle |\mathcal{N}_{\mathcal{B}}\rangle, \quad (19)$$

where $|n_{\mathcal{B}}\rangle$ is a Fock state of the bath with n photons and \mathcal{N} is the total number of incident photons. Our calculation only considers the state without loss, $|\psi_{\text{out}}\rangle \equiv |\theta_0\rangle$, which is not normalized as seen from Eq. (19). The density operator is $\hat{\rho} = |\Theta\rangle\langle\Theta|$ and the reduced density operator is found by tracing out the bath

$$\hat{\rho}_s = \text{Tr}_{\text{bath}}[\hat{\rho}] = \sum_{m_{\mathcal{B}}=0}^{\mathcal{N}} \langle m_{\mathcal{B}} | \hat{\rho} | m_{\mathcal{B}} \rangle = \sum_{n=0}^{\mathcal{N}} |\theta_n\rangle\langle\theta_n|. \quad (20)$$

If $|\mu_0\rangle$ is the desired output state, the state fidelity is defined as [42]

$$\mathcal{F}_s \equiv \langle \mu_0 | \hat{\rho}_s | \mu_0 \rangle = |\langle \mu_0 | \psi_{\text{out}} \rangle|^2 + \sum_{n=1}^{\mathcal{N}} |\langle \mu_0 | \theta_n \rangle|^2. \quad (21)$$

If we denote the unnormalized (no-loss) output state (the output state that we calculate) when there are \mathcal{N} input photons by $|\psi_{\text{out}}^{(\mathcal{N})}\rangle$, and define the “ \mathcal{N} -photon state fidelity” by

$$\langle \mu_0 | \psi_{\text{out}}^{(\mathcal{N})} \rangle = \sqrt{F_{\mathcal{N}}} e^{i\vartheta_n}, \quad (22)$$

then $F_{\mathcal{N}}$ is a lower bound on the fidelity, \mathcal{F}_s , as seen from Eq. (21).

The one- and two-photon output states are given by

$$|\psi_{\text{out}}^{(1)}\rangle = \int_{t_0}^{t_N} dt \xi_{\text{out}}(t) \hat{w}^\dagger(t) |\emptyset\rangle, \quad (23a)$$

$$|\psi_{\text{out}}^{(2)}\rangle = \int_{t_0}^{t_N} \int_{t_0}^{t_N} dt_m dt_n \xi_{\text{out}}(t_m, t_n) \hat{w}^\dagger(t_m) \hat{w}^\dagger(t_n) |\emptyset\rangle, \quad (23b)$$

so that the overlaps in Eq. (22) are

$$\langle \mu_0 | \psi_{\text{out}}^{(1)} \rangle = \int_{t_0}^{t_N} \xi_{\text{out}}(t) \xi_\mu(t)^* dt, \quad (24)$$

$$\langle \mu_0 | \psi_{\text{out}}^{(2)} \rangle = \int_{t_0}^{t_N} \int_{t_0}^{t_N} \xi_{\text{out}}(t_m, t_n) \xi_\mu(t_n)^* \xi_\mu(t_m)^* dt_m dt_n, \quad (25)$$

where we have assumed that $|\mu_0\rangle$ for two-photon inputs is a separable state with a wave packet, $\xi_\mu(t)$.

If it is known that all input photons were present in the output state (such knowledge could be obtained by detection), it corresponds to projecting the state $|\Theta\rangle$ onto the zero-loss subspace

$$|\Theta_P\rangle = \frac{(|0_B\rangle\langle 0_B|)|\Theta\rangle}{\sqrt{\langle \Theta | (|0_B\rangle\langle 0_B|) | \Theta \rangle}} = \frac{|\psi_{\text{out}}\rangle |0_B\rangle}{\sqrt{\langle \psi_{\text{out}} | \psi_{\text{out}} \rangle}}. \quad (26)$$

The probability of losing at least one photon is $P_L = 1 - \langle \psi_{\text{out}} | \psi_{\text{out}} \rangle$. If we define the projected state of the considered system as the renormalized state, $|\psi_P\rangle = |\psi_{\text{out}}\rangle / \langle \psi_{\text{out}} | \psi_{\text{out}} \rangle$, it may be understood as the output state conditioned on the knowledge that no photons were lost. We may then define the conditional fidelity

$$\bar{F}_{\mathcal{N}} \equiv |\langle \mu_0 | \psi_P^{(\mathcal{N})} \rangle|^2 = \frac{F_{\mathcal{N}}}{1 - P_L}, \quad (27)$$

Eq. (27) may be interpreted using Baye’s rule, $P(A|B) = P(A, B)/P(B)$, where A means “ ξ_μ and ξ_{out} have the same shape” and B means “no photons were lost.” $\bar{F}_{\mathcal{N}}$ is useful because it determines the visibility of quantum interference between output photons and other photons that did not scatter off a dynamically coupled cavity.

Since the calculation of $|\psi_{\text{out}}\rangle$ leads to a lower bound on the fidelity of output states, we simply include the loss term proportional to γ_L in all the equations of motion in the following sections.

C. Two cavity modes and one photon

For two cavity modes and a $\chi^{(3)}$ material, the Hamiltonian describing the linear dynamics is

$$\begin{aligned} \hat{H}_n^{(2)} = & \hbar \delta_a \hat{a}^\dagger \hat{a} + \hbar \delta_b \hat{b}^\dagger \hat{b} + i \hbar \sqrt{\frac{\gamma}{\Delta t}} (\hat{a}^\dagger \hat{w}_n - \hat{a} \hat{w}_n^\dagger) \\ & + \hbar (\Lambda_n^* \hat{a}^\dagger \hat{b} + \Lambda_n \hat{b}^\dagger \hat{a}) + 2 \hbar |\Lambda_n| (\hat{a}^\dagger \hat{a} + \hat{b}^\dagger \hat{b}). \end{aligned} \quad (28)$$

The corresponding time-evolution operator is

$$\begin{aligned} \hat{U}_n^{(2)} \approx & \hat{\mathbb{1}} + \sqrt{\gamma \Delta t} (\hat{a}^\dagger \hat{w}_n - \hat{a} \hat{w}_n^\dagger) - \frac{\gamma}{2} \Delta t \hat{a}^\dagger \hat{a} \hat{w}_n \hat{w}_n^\dagger \\ & - i \Delta t (\Lambda_n^* \hat{a}^\dagger \hat{b} + \Lambda_n \hat{b}^\dagger \hat{a}) - i \Delta t (\delta_a + 2 |\Lambda_n|) \hat{a}^\dagger \hat{a} \\ & - i \Delta t (\delta_b + 2 |\Lambda_n|) \hat{b}^\dagger \hat{b}. \end{aligned} \quad (29)$$

Note that we have omitted the loss terms from Eq. (18), but we will include them in the equations of motion below. The state at time step n is

$$\begin{aligned} |\psi_n\rangle = & \sum_{k=n+1}^N \xi_k^{\text{in}} \sqrt{\Delta t} |00\rangle |1_k\rangle + \sum_{k=1}^n \xi_k^{\text{out}} \sqrt{\Delta t} |00\rangle |1_k\rangle \\ & + \psi_{10}(n) |10\rangle |\emptyset\rangle + \psi_{01}(n) |01\rangle |\emptyset\rangle, \end{aligned} \quad (30)$$

where $|01\rangle \equiv |0_a\rangle |1_b\rangle$ is the state with one photon in mode b . In Appendix C, we derive the equations of motion for the coefficients $\psi_{10}(t)$ and $\psi_{01}(t)$ along with the input-output relation

$$\dot{\psi}_{10} = - \left(i \delta_a + \frac{\Gamma}{2} + i 2 |\Lambda| \right) \psi_{10} - i \Lambda^* \psi_{01} + \sqrt{\gamma} \xi_{\text{in}}, \quad (31a)$$

$$\dot{\psi}_{01} = - \left(i \delta_b + \frac{\gamma_L}{2} + i 2 |\Lambda| \right) \psi_{01} - i \Lambda \psi_{10}, \quad (31b)$$

$$\xi_{\text{out}} = \xi_{\text{in}} - \sqrt{\gamma} \psi_{10}. \quad (31c)$$

Note that we have not explicitly written the time dependence of the functions in Eq. (31).

D. Two cavity modes and two identical photons

The analysis becomes significantly more complicated for two input photons, so we find it beneficial to map out all the different paths they may take from input to output and the different types of states generated in the process; see Fig. 3. Let us go through the layers of the map from left to right and write down the dynamical equations governing the Schrödinger coefficients of the states in each layer. The first layer only contains the input state

$$|\psi_0\rangle = \sqrt{2} \sum_{j=1}^N \sum_{k>j}^N \xi_j^{\text{in}} \xi_k^{\text{in}} \Delta t |00\rangle |1_j 1_k\rangle. \quad (32)$$

Note that the summation over k starts at j in Eq. (32) so that the indistinguishable states $|1_j 1_k\rangle$ and $|1_k 1_j\rangle$ are only counted once in the summations. In Appendix D, we prove that the factor of $\sqrt{2}$ ensures that the state is normalized when the integral of $|\xi_{\text{in}}(t)|^2$ equals 1. We note that derivations of all the equations of motion for coefficients of the Schrödinger picture state in this section may be found in Appendix D.

One of the two photons in layer 1 may be absorbed giving rise to states in layer 2 with one photon in mode a or b . The dynamical equations for the coefficients corresponding to these states are

$$\dot{\psi}_{10}^{(2)} = - \left(i \delta_a + \frac{\Gamma}{2} + i 2 |\Lambda| \right) \psi_{10}^{(2)} - i \Lambda^* \psi_{01}^{(2)} + \sqrt{2} \sqrt{\gamma} \xi_{\text{in}}, \quad (33a)$$

$$\dot{\psi}_{01}^{(2)} = - \left(i \delta_b + \frac{\gamma_L}{2} + i 2 |\Lambda| \right) \psi_{01}^{(2)} - i \Lambda \psi_{10}^{(2)}, \quad (33b)$$

where we use the superscript (2) to signify that the driving term in Eq. (33a) originates from two input photons, which

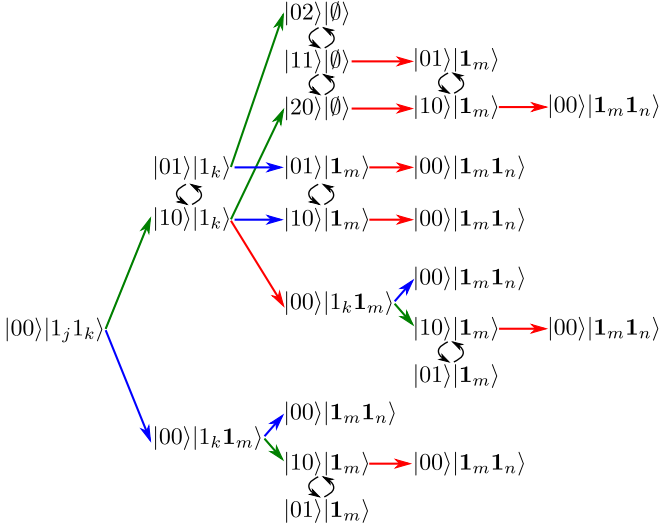


FIG. 3. Map of states generated with two cavity modes and two input photons and paths from input to output. Green arrows represent absorption of a photon into mode a . Red arrows represent emission into the waveguide in bin m . Blue arrows represent a photon passing by the system without interacting in time bin m . Black arrows indicate the interaction between modes a and b driven by the external control fields. There are five vertical layers going from left to right.

is why it contains a factor of $\sqrt{2}$ relative to Eq. (31a). A convenient feature of the map in Fig. 3 is that the couplings represented by black arrows turn up in the equations of motion as coupling terms proportional to the control field, $\Lambda(t)$, and therefore serves to check whether all the dynamics is included.

The state $|00\rangle|1_k\mathbf{1}_m\rangle$ in layer 2 originates from direct passage of one of the input photons at time t_m , while in layer 3 it originates from absorption and subsequent emission. If the photon remaining on the input side is later absorbed, it gives rise to states $|10\rangle|\mathbf{1}_m\rangle$ and $|01\rangle|\mathbf{1}_m\rangle$ in layer 3 or 4. The dynamical equations for the coefficients corresponding to these states are

$$\dot{\psi}_{10}^{(1)}(t_m, t) = -\left[i\delta_a + \frac{\Gamma}{2} + i2|\Lambda(t)|\right]\psi_{10}^{(1)}(t_m, t) - i\Lambda^*\psi_{01}^{(1)}(t_m, t) + \sqrt{\gamma}\xi_{\text{in}}(t) \quad (34a)$$

$$\dot{\psi}_{01}^{(1)}(t_m, t) = -\left[i\delta_b + \frac{\gamma_L}{2} + i2|\Lambda(t)|\right]\psi_{01}^{(1)}(t_m, t) - i\Lambda\psi_{10}^{(1)}(t_m, t), \quad (34b)$$

where the superscript (1) signifies that Eq. (34a) is driven by a single input photon. The coefficients $\psi_{10}^{(1)}$ and $\psi_{01}^{(1)}$ are functions of two times, t_m being the initial time at which the state $|00\rangle|1_k\mathbf{1}_m\rangle$ was created and $t \geq t_m$ describing the subsequent evolution of the coefficients. The initial condition of Eq. (34) is $\psi_{10}^{(1)}(t_m, t_m) = \psi_{01}^{(1)}(t_m, t_m) = 0$ since the system is in state $|00\rangle$ at time t_m .

States in layer 3 with two photons in the system have coefficients with the following equations of motion:

$$\dot{\psi}_{20} = -(i2\delta_a + \Gamma + i4|\Lambda|)\psi_{20} - i\sqrt{2}\Lambda^*\psi_{11} + \sqrt{2\gamma}\psi_{10}^{(2)}\xi_{\text{in}}, \quad (35a)$$

$$\dot{\psi}_{11} = -\left[i(\delta_a + \delta_b) + \frac{\Gamma + \gamma_L}{2} + i4|\Lambda|\right]\psi_{11} - i\sqrt{2}(\Lambda\psi_{20} + \Lambda^*\psi_{02}) + \sqrt{\gamma}\psi_{01}^{(2)}\xi_{\text{in}}, \quad (35b)$$

$$\dot{\psi}_{02} = -(i2\delta_b + \gamma_L + i4|\Lambda|)\psi_{02} - i\sqrt{2}\Lambda\psi_{11}. \quad (35c)$$

The initial conditions are $\psi_{20}(0) = \psi_{11}(0) = \psi_{02}(0) = 0$.

There are other paths leading to the states $|10\rangle|\mathbf{1}_m\rangle$ and $|01\rangle|\mathbf{1}_m\rangle$ than those described by the dynamics in Eq. (34). It could either be from absorption of the first photon followed by direct passage of the second photon or emission from mode a while the state is $|20\rangle|\emptyset\rangle$ or $|11\rangle|\emptyset\rangle$. We use different coefficients for the state originating from these paths because their dynamical equations do not contain driving terms from input photons

$$\dot{\psi}_{10}^{(0)}(t_m, t) = -\left[i\delta_a + \frac{\Gamma}{2} + i2|\Lambda(t)|\right]\psi_{10}^{(0)}(t_m, t) - i\Lambda(t)^*\psi_{01}^{(0)}(t_m, t), \quad (36a)$$

$$\dot{\psi}_{01}^{(0)}(t_m, t) = -\left[i\delta_b + \frac{\gamma_L}{2} + i2|\Lambda(t)|\right]\psi_{01}^{(0)}(t_m, t) - i\Lambda(t)\psi_{10}^{(0)}(t_m, t). \quad (36b)$$

There are two sets of initial conditions for Eq. (36) depending on whether the dynamics originated from the formation of state $|10\rangle|\mathbf{1}_m\rangle$ or $|01\rangle|\mathbf{1}_m\rangle$ at time t_m . If the photon started in mode a , the initial condition is $\psi_{10}^{(0)}(t_m, t_m) = 1$ and $\psi_{01}^{(0)}(t_m, t_m) = 0$, and we define $A_{10} \equiv \psi_{10}^{(0)}$ and $A_{01} \equiv \psi_{01}^{(0)}$. If the photon started in mode b , the initial condition is $\psi_{10}^{(0)}(t_m, t_m) = 0$ and $\psi_{01}^{(0)}(t_m, t_m) = 1$, and we define $B_{10} \equiv \psi_{10}^{(0)}$ and $B_{01} \equiv \psi_{01}^{(0)}$.

Figure 3 reveals that there are eight distinct paths from input to output so the coefficient of the output state, $|00\rangle|\mathbf{1}_m\mathbf{1}_n\rangle$, should contain eight terms:

$$\begin{aligned} \xi_{\text{out}}(t_m, t) &= \frac{1}{\sqrt{2}}[\gamma\psi_{11}(t_m)B_{10}(t_m, t) + \sqrt{2\gamma}\psi_{20}(t_m)A_{10}(t_m, t) \\ &\quad - \sqrt{\gamma}\psi_{01}^{(2)}(t_m)\xi(t_m)B_{10}(t_m, t) \\ &\quad - \sqrt{\gamma}\psi_{10}^{(2)}(t_m)\xi(t_m)A_{10}(t_m, t) - \sqrt{\gamma}\psi_{10}^{(2)}(t_m)\xi(t) \\ &\quad + \gamma\psi_{10}^{(2)}(t_m)\psi_{10}^{(1)}(t_m, t) + \sqrt{2}\xi(t_m)\xi(t) \\ &\quad - \sqrt{2\gamma}\xi(t_m)\psi_{10}^{(1)}(t_m, t)], \end{aligned} \quad (37)$$

where we omitted the subscript of ξ_{in} for brevity. The first term in Eq. (37) corresponds to the upper path in Fig. 3, the second term to the path immediately below, and so forth. Note that $t_m \leq t$ in Eq. (37) and $\xi_{\text{out}}(t_m, t) = \xi_{\text{out}}(t, t_m)$ follows from the indistinguishability of the photons. To calculate the output state in Eq. (37), we solve the above equations of motion for N different initial conditions corresponding to all the time bins in Fig. 2.

V. ABSORBING AND EMITTING WAVE PACKETS VIA DYNAMIC COUPLING

In this section, we find analytic solutions for the control fields that allow absorption and emission of wave packets

with known shapes. We consider a specific example of Gaussian wave packets and show by numerical integration of Eq. (31) that the fidelity of the absorption and emission process approaches unity very rapidly as the ratio between the cavity-waveguide coupling, γ , and the wave packet bandwidth, Ω_G , increases.

A. Absorption

For the absorption process, the initial condition of Eq. (31) is $\psi_{10}(t_0) = \psi_{01}(t_0) = 0$. We use a subscript i (for *in*) on the control function, $\Lambda_i(t)$. The goal is to determine $\Lambda_i(t)$ such that a single incoming photon with wave packet $\xi_{in}(t)$ is absorbed into cavity mode b . Since Λ_i is complex valued, we write it as $\Lambda_i(t) = |\Lambda_i(t)| \exp[i\phi_i(t)]$. In Appendix E, we find the solution for a material with a third-order nonlinearity:

$$|\Lambda_i(t)| = \frac{|f_i(t)|e^{-\frac{\gamma t}{2}}}{|\xi_{in}(t)|\sqrt{2\int_{t_0}^t f_i(s)ds - 4|\xi_{in}(t)|^2 e^{\gamma t}}}, \quad (38a)$$

$$\begin{aligned} \phi_i(t) = & -\delta_b t - 2\int_{t_0}^t |\Lambda_i(s)|ds - \arg(\xi_{in}) \\ & + \tan^{-1}\left[\frac{f_i \sin(\theta_i) - g_i \cos(\theta_i)}{f_i \cos(\theta_i) + g_i \sin(\theta_i)}\right], \end{aligned} \quad (38b)$$

where

$$f_i(t) = \left[\frac{\gamma - \gamma_L}{2}\xi_{in}(t) - \dot{\xi}_{in}(t)\right]\xi_{in}(t)^* e^{\gamma t}, \quad (39a)$$

$$g_i(t) = -2|\Lambda_i(t)||\xi_{in}(t)|^2 e^{\gamma t}, \quad (39b)$$

$$\theta_i(t) = -\frac{1}{2}\int_{t_0}^t \frac{g_i(s)}{\int_{t_0}^s f_i(z)dz} ds. \quad (39c)$$

Note that we have assumed that ξ_{in} does not have a time-dependent phase, such that f_i and g_i are real functions. It is straightforward to generalize this to chirped pulses with time-dependent phases by redefining f_i and g_i . We also assumed $\delta_a = 0$ above.

In the case of a material with a second-order nonlinearity, there is no cross-phase modulation from the control field, so $g_i = 0$ and the solution reduces to

$$|\Lambda_i(t)| = \frac{|f_i(t)|e^{-\frac{\gamma t}{2}}}{|\xi_{in}(t)|\sqrt{2\int_{t_0}^t f_i(s)ds}}, \quad (40a)$$

$$\phi_i(t) = -\delta_b t - \arg(\xi_{in}), \quad (40b)$$

with $f_i(t)$ still given by Eq. (39a).

B. Emission

Without any driving field, the equations of motion are found by setting $\xi_{in} = 0$ in Eq. (31)

$$\dot{\psi}_{10} = \left(-\frac{\Gamma}{2} - i2|\Lambda_o|\right)\psi_{10} - i|\Lambda_o|e^{-i\phi_o}\psi_{01}, \quad (41a)$$

$$\dot{\psi}_{01} = \left(-\frac{\gamma_L}{2} - i2|\Lambda_o|\right)\psi_{01} - i|\Lambda_o|e^{i\phi_o}\psi_{10}, \quad (41b)$$

$$\dot{\xi}_{out} = -\sqrt{\gamma}\psi_{10}. \quad (41c)$$

Note that we use the subscript o (for *out*) on the control function in Eq. (41). The initial condition is $\psi_{10}(t_0) = 0$ and state $|01\rangle|\emptyset\rangle$ has the complex amplitude $\psi_{01}(t_0)$. The goal is to determine $|\Lambda_o(t)|$ and $\phi_o(t)$ such that $\xi_{out}(t)$ equals some desired wave packet, $\xi(t)$. The solution is found in Appendix F:

$$|\Lambda_o(t)| = \frac{|f_o|e^{-\frac{\gamma t}{2}}}{|\xi|\sqrt{\gamma|\psi_{01}(t_0)|^2 - 2\int_{t_0}^t f_o(s)ds - 4|\xi|^2 e^{\gamma t}}}, \quad (42a)$$

$$\begin{aligned} \phi_o(t) = & -\delta_b t - 2\int_{t_0}^t |\Lambda_o(s)|ds - \arg(\xi) \\ & + \tan^{-1}\left[\frac{f_o \cos(\theta_o) - g_o \sin(\theta_o)}{-f_o \sin(\theta_o) - g_o \cos(\theta_o)}\right], \end{aligned} \quad (42b)$$

where

$$f_o(t) = \left[\frac{\Gamma}{2}\xi(t) + \dot{\xi}(t)\right]\xi(t)^* e^{\gamma t}, \quad (43a)$$

$$g_o(t) = -2|\Lambda_o(t)||\xi(t)|^2 e^{\gamma t}, \quad (43b)$$

$$\theta_o(t) = -\int_{t_0}^t \frac{g_o(s)}{\gamma|\psi_{01}(0)|^2 - 2\int_{t_0}^s f_o(z)dz} ds. \quad (43c)$$

Again, we assumed $\delta_a = 0$.

The solution simplifies in the case of a material with a second-order nonlinearity,

$$|\Lambda_o(t)| = \frac{|f_o|e^{-\frac{\gamma t}{2}}}{|\xi|\sqrt{\gamma|\psi_{01}(t_0)|^2 - 2\int_{t_0}^t f_o(s)ds}}, \quad (44a)$$

$$\phi_o(t) = -\delta_b t - \arg(\xi) - \frac{\pi}{2}, \quad (44b)$$

with $f_o(t)$ still given by Eq. (43a).

We note that the solutions found in this section correspond to the amplitude and phase of control fields inside the cavity. In Appendix G, we derive expressions for the control fields in the waveguide giving rise to these desired cavity fields.

C. Gaussian wave packet

We consider an example of a Gaussian wave packet to investigate how well our absorption and emission technique works. The Gaussian wave packet of the input field is defined as

$$\mathcal{G}(t) = \sqrt{\frac{2}{\tau_G} \left[\frac{\ln(2)}{\pi}\right]^{\frac{1}{4}}} \exp\left[-2\ln(2)\frac{t^2}{\tau_G^2}\right], \quad (45)$$

where $|\mathcal{G}(t)|^2$ has a full temporal width at half maximum (FWHM) of τ_G , spectral width of $\Omega_G = 4\ln(2)/\tau_G$, and integrates to 1 (over the infinite interval from $-\infty$ to ∞). The input states are characterized by the wave packet $\xi_{in}(t) = \mathcal{G}(t - T_i)$ and the ideal output state is characterized by a simple time translation

$$|\mathcal{G}_{out}\rangle = \int_{t_0}^{t_N} dt \mathcal{G}(t - T_o)\hat{w}^\dagger(t)|\emptyset\rangle, \quad (46)$$

where $T_o = T_i + T$ and T is the storage time. The duration of the entire interaction process, $t_N = T_o + \tau_o$, is divided into three time intervals denoted *absorption*, $t \in [0, 2T_i]$, *storage*, $t \in [2T_i, T_o - \tau_o]$, and *emission*, $t \in [T_o - \tau_o, t_N]$. Practically, wave packets must have a finite duration and our choice of

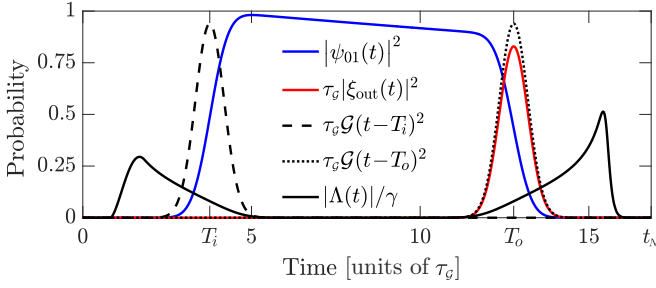


FIG. 4. Plots of the solution to Eq. (31) along with the input-output Gaussians and the control field found in Eqs. (38a) and (42a). Parameters: $\gamma/\Omega_G = 30$, $\gamma_L/\Omega_G = 5 \times 10^{-3}$, $\tau_e = \tau_G$, $\tau_o/\tau_G = 4.08$, $T/\tau_G = 9$.

absorption interval causes a discontinuous jump in ξ_{in} from $\xi_{in}(0^-) = 0$ to $\xi_{in}(0^+) = \mathcal{G}(-T_i)$. The field in cavity mode a takes a finite time to build up sufficiently to cause complete destructive interference with the part of the incoming wave packet that did not interact with the cavity. It is therefore impossible to perfectly absorb a wave packet of finite length, but the probability that the photon passes by the cavity without interacting, P_{pass} , becomes negligible for relatively small values of the ratio γ/Ω_G as seen below. The problem of absorbing a wave packet of finite length is reflected in the solutions for the control fields in Eqs. (38a) and (42a), which become imaginary when the terms under the square root in the denominators are negative. As explained in Appendix F 1, we use smoothing functions to avoid divergences and ensure the control functions are zero outside the absorption and emission intervals. The smoothing functions in Eq. (F24) are parametrized by the on-off duration, τ_e .

Figure 4 shows an example of the absorption, storage, and emission of a single photon in a Gaussian wave packet. The control field is given by $\Lambda = \Lambda_i + \Lambda_o$ since the storage time, T , is chosen large enough to avoid overlap between the absorption and emission intervals, $T > T_i + \tau_o$. Note that the control field responsible for emission is different from a simple time inversion of the control field responsible for absorption. This is because the presence of loss breaks the time-reversal symmetry of the equations of motion in Eq. (31).

In the presence of loss, it is possible to emit a wave packet with the desired shape but reduced amplitude, $\xi_{out}(t) \approx \sqrt{\eta} \mathcal{G}(t - T_o)$, where η is a real number smaller than 1. Note, however, that this is only true in the emission interval, $t \in [T_o - \tau_o, t_v]$, since $\xi_{out}(t)$ generally has some small contribution from the absorption interval due to imperfect absorption. The probability that the photon passes by the cavity without being absorbed is

$$P_{pass} \equiv \int_{t_0}^{2T_i} |\xi_{out}(t)|^2 dt. \quad (47)$$

The probability of a successful storage process is equal to η in the limit $P_{pass} \rightarrow 0$. The maximum possible value of η can be found by inserting $\xi = \sqrt{\eta} \mathcal{G}$ into the denominator of Eq. (42a) and ensuring that the terms under the square root are positive for all t . For the Gaussian in Eq. (45), we have

$$\mathcal{F}_o \equiv 2 \int_{-\infty}^{\infty} f_o(t) dt = \gamma \exp \left\{ \gamma_L \left[T_o + \frac{\gamma_L \tau_G^2}{16 \ln(2)} \right] \right\}, \quad (48)$$

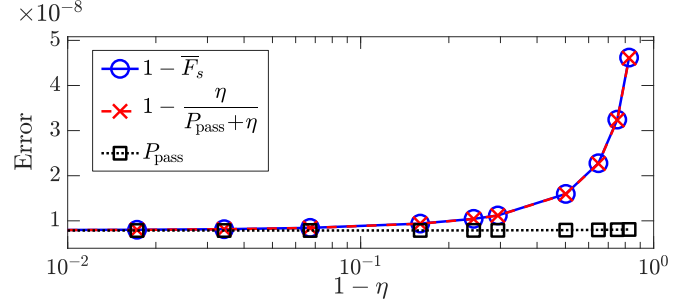


FIG. 5. Degradation of conditional fidelity in the limit of large loss. Parameters: $\gamma/\Omega_G = 30$, $\tau_e = \tau_G$.

and we therefore choose η as

$$\eta = \frac{\gamma |\psi_{01}(t_0)|^2}{\mathcal{F}_o} (1 - \epsilon_\eta). \quad (49)$$

The value of the small parameter, ϵ_η , is optimized by minimizing $|\psi_{01}(t_v)|^2$, which is the probability that an absorbed photon remains in mode b after the emission interval. Finite values of P_{pass} limits the achievable overlap of the output wave packet with a desired shape, which is seen by calculating the conditional fidelity in Eq. (27) using $\xi_{out} = \sqrt{\eta} \mathcal{G}(t - T_o)$ in the emission interval

$$\bar{F}_1 = \frac{\left| \int_{t_0}^{t_v} \xi_{out}(t) \mathcal{G}(t - T_o)^* dt \right|^2}{\int_{t_0}^{t_v} |\xi_{out}(t)|^2 dt} \approx \frac{\eta}{P_{pass} + \eta}, \quad (50)$$

where we changed the lower integration limit from t_0 to $T_o - \tau_o$ in the numerator since $\mathcal{G}(t - T_o) \approx 0$ outside the emission interval. We also divided the integration of $|\xi_{out}|^2$ into intervals $[0, 2T_i]$ and $[T_o - \tau_o, t_v]$ since $|\xi_{out}(t)|^2 \approx 0$ in the storage interval. Figure 5 shows a plot of the conditional fidelity using ξ_{out} calculated from Eq. (31) along with the approximation in Eq. (50). It also shows that $\bar{F}_1 \rightarrow 1 - P_{pass}$ in the limit where $P_{pass} \ll \eta$ and $\eta \approx 1$, which is seen from a Taylor expansion of Eq. (50), $\bar{F}_1 \approx 1/(1 + P_{pass}/\eta) \approx 1 - P_{pass}/\eta$. It is important to note that Fig. 5 clearly illustrates that very small error in the conditional fidelity is possible even in the case of an efficiency well below unity.

The value of P_{pass} only depends on the ratio γ/Ω_G and Fig. 6 plots the dependence for both second- and third-order nonlinear materials. It is seen that P_{pass} falls off more quickly for $\chi^{(2)}$ materials due to the absence of cross-phase modula-

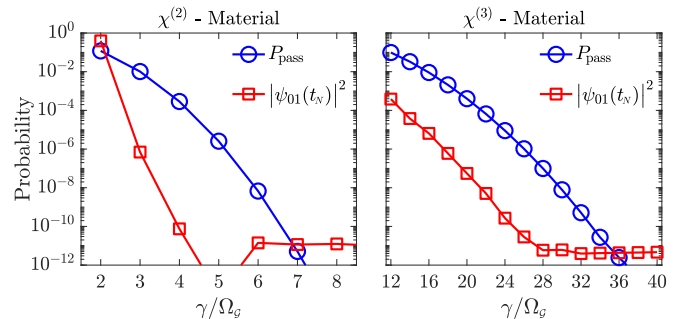


FIG. 6. P_{pass} as a function of γ/Ω_G for $\chi^{(2)}$ and $\chi^{(3)}$ materials. Parameters: $\gamma_L = 0$, $\tau_e = \tau_G$.

tion. In Appendix E 1, we derive expressions suggesting that a five times larger coupling rate, γ , is needed for a $\chi^{(3)}$ material, which agrees well with the result in Fig. 6. Importantly, Fig. 6 shows that P_{pass} approaches zero extremely fast as the ratio γ/Ω_G increases.

VI. NONLINEAR DYNAMICS

In this section, we consider three types of nonlinearities that mediate photon-photon interactions and describe the necessary extensions to the equations of motion in Sec. IV to account for them. Since we have a particular interest in two-qubit logic gates for quantum information processing, we consider cavity configurations enabling a C-phase gate. Note that we envision a configuration where two identical cavities are placed in between two 50:50 beam splitters that convert the two-qubit state $|11\rangle$ into $1/\sqrt{2}(|02\rangle + |20\rangle)$ [43,44]. In this case, the phase ϑ_n in Eq. (22) is important in that $\vartheta_2 - 2\vartheta_1 = \pi$ is required for the gate transformation $|00\rangle \rightarrow |00\rangle$, $|10\rangle \rightarrow |10\rangle$, $|01\rangle \rightarrow |01\rangle$, $|11\rangle \rightarrow -|11\rangle$. For a more complete analysis of gate performance, we refer to Ref. [45].

We start by considering a material with a third-order nonlinearity, then we describe second-order nonlinearities, and finally interactions with a two-level emitter. In all numerical examples we use the Gaussian input wave packet in Eq. (45).

A. Material with a third-order nonlinearity

Only modes a and b are needed in the case of a $\chi^{(3)}$ material. The Hamiltonian corresponding to photon-photon interactions is

$$\hat{H}_{\chi^{(3)}} = \hbar\chi_3 \left[\hat{a}^\dagger \hat{a} \hat{b}^\dagger \hat{b} + \frac{(\hat{a}^\dagger \hat{a} - 1)\hat{a}^\dagger \hat{a} + (\hat{b}^\dagger \hat{b} - 1)\hat{b}^\dagger \hat{b}}{4} \right]. \quad (51)$$

The corresponding unitary time-evolution operator is

$$\begin{aligned} \hat{U}_{\chi^{(3)}} &= -i\Delta t \chi_3 \hat{b}^\dagger \hat{b} \hat{a}^\dagger \hat{a} \\ &\quad - i\frac{1}{4}\Delta t \chi_3 [(\hat{b}^\dagger \hat{b} - 1)\hat{b}^\dagger \hat{b} + (\hat{a}^\dagger \hat{a} - 1)\hat{a}^\dagger \hat{a}]. \end{aligned} \quad (52)$$

Only states with two photons in the system are affected, so that

$$\hat{U}_{\chi^{(3)}}|20\rangle = -i\chi_3 \Delta t \frac{1}{4}(2-1)2|20\rangle = -i\frac{\chi_3}{2}\Delta t|20\rangle, \quad (53a)$$

$$\hat{U}_{\chi^{(3)}}|11\rangle = -i\chi_3 \Delta t|11\rangle, \quad (53b)$$

$$\hat{U}_{\chi^{(3)}}|02\rangle = -i\chi_3 \Delta t \frac{1}{4}(2-1)2|02\rangle = -i\frac{\chi_3}{2}\Delta t|02\rangle. \quad (53c)$$

The equations of motion for the corresponding coefficients in Eq. (35) are therefore modified as

$$\begin{aligned} \dot{\psi}_{20} &= -\left(i2\delta_a + \Gamma + i\frac{\chi_3}{2} + i4|\Lambda|\right)\psi_{20} - i\sqrt{2}\Lambda^*\psi_{11} \\ &\quad + \sqrt{2\gamma}\psi_{10}^{(2)}\xi_{\text{in}}, \end{aligned} \quad (54a)$$

$$\begin{aligned} \dot{\psi}_{11} &= -\left(i(\delta_a + \delta_b) + \frac{\Gamma + \gamma_L}{2} + i\chi_3 + i4|\Lambda|\right)\psi_{11} \\ &\quad - i\sqrt{2}[\Lambda\psi_{20} + \Lambda^*\psi_{02}] + \sqrt{\gamma}\psi_{01}^{(2)}\xi_{\text{in}}, \end{aligned} \quad (54b)$$

$$\dot{\psi}_{02} = -\left(i2\delta_b + \gamma_L + i\frac{\chi_3}{2} + i4|\Lambda|\right)\psi_{02} - i\sqrt{2}\Lambda\psi_{11}. \quad (54c)$$

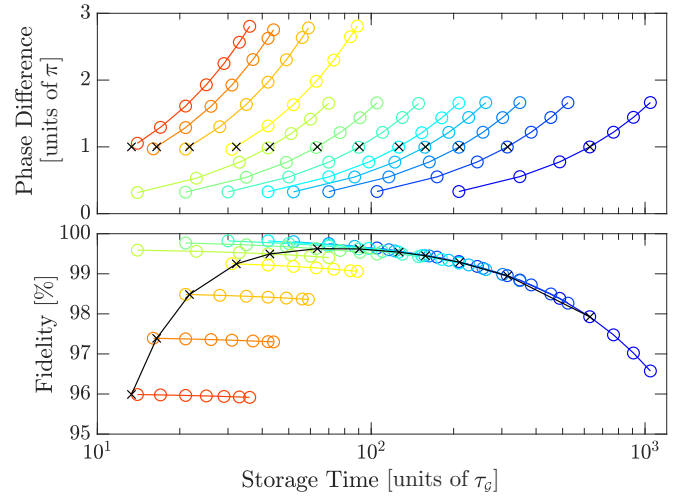


FIG. 7. Nonlinear phase difference, $\Delta\vartheta$, and fidelity, F_2 , as a function of storage time for different values of the nonlinear coupling rate, χ_3 , ranging from $0.01\Omega_G$ (blue) to $0.5\Omega_G$ (red). The black line shows the fidelity corresponding to $\Delta\vartheta = \pi$. Parameters: $\gamma/\Omega_G = 30$, $\gamma_L/\Omega_G = 10^{-5}$, $\tau_c = \tau_G$.

It is seen from Eq. (54c) that the amplitude of the state $|02\rangle$ acquires a phase proportional to $\chi_3/2$, which the amplitude of the state $|01\rangle$ in Eq. (31b) does not. By a careful choice of storage time, T , one may achieve the condition $\Delta\vartheta = \vartheta_2 - 2\vartheta_1 = \pi$, where ϑ_n is the phase in Eq. (22). Figure 7 plots the phase difference as a function of storage time for a range of different nonlinear coupling coefficients, χ_3 . It shows how the phase condition, $\Delta\vartheta = \pi$, may be met using a smaller nonlinearity and larger storage time (blue curve) or a larger nonlinearity and smaller storage time (red curve). Figure 7 also plots the corresponding fidelity, F_2 , which appears to reach an optimum for $T/\tau_G \approx 100$. The fidelity degrades when increasing χ_3 because the solutions for the control fields were found assuming a single-photon input and photon-photon interactions during the absorption and emission process renders the control fields suboptimal. The fidelity also degrades if χ_3 is decreased too much because losses increase with increased storage time.

B. Material with a second-order nonlinearity

For materials exhibiting a $\chi^{(2)}$ nonlinearity, we explore the process of second harmonic generation where $\omega_c = 2\omega_b$. With the introduction of mode c , the system states are written as $|n_a n_b n_c\rangle$ with n_a , n_b , and n_c representing the number of photons in each mode. The Hamiltonian describing the interaction is given in Eq. (13b). The corresponding unitary time-evolution operator is

$$\hat{U}_{\text{SHG}} = -i\chi_2 \Delta t (\hat{c} \hat{b}^\dagger \hat{b}^\dagger + \hat{c}^\dagger \hat{b} \hat{b}). \quad (55)$$

From Eq. (55), we see that it only causes a coupling between states $|020\rangle$ and $|001\rangle$

$$\hat{U}_{\text{SHG}}|020\rangle = -i\chi_2 \Delta t \sqrt{2}|001\rangle, \quad (56a)$$

$$\hat{U}_{\text{SHG}}|001\rangle = -i\chi_2 \Delta t \sqrt{2}|020\rangle. \quad (56b)$$

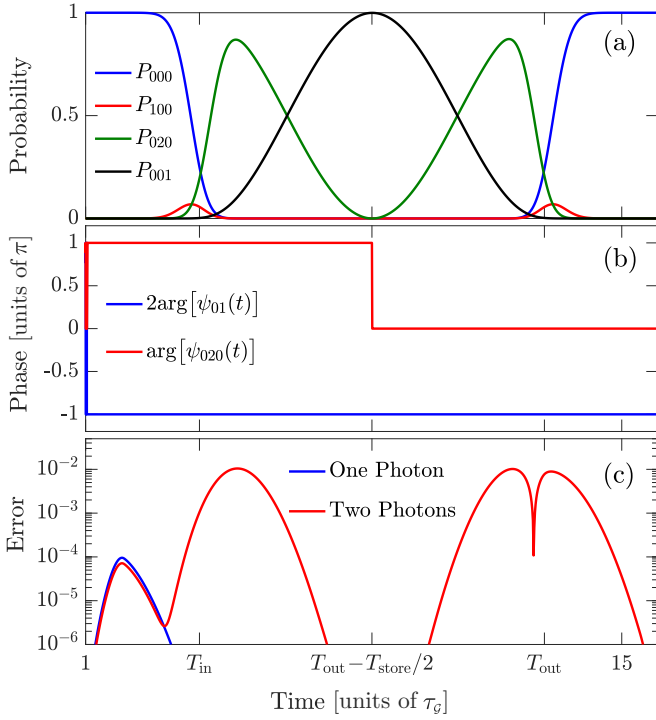


FIG. 8. (a) Occupation probabilities of system states as a function of time. (b) Phase of the coefficient corresponding to state $|01\rangle$ (blue) and $|020\rangle$ (red). (c) Error measured as the absolute distance from a Gaussian, $|\xi_{out}(t) - \sqrt{\eta}\mathcal{G}(t - T_o)|$ (blue) and $|\xi_{out}(t_m, T_o) + \eta\mathcal{G}(t_m - T_o)\mathcal{G}(0)|$ (red). Parameters: $\gamma/\Omega_G = 6\Omega_G$, $\gamma_L/\Omega_G = 1.5 \times 10^{-4}$, $\tau_e = \tau_G$, $\eta = 0.9963$.

The equations of motion for coefficients corresponding to two photons in the system are then

$$\dot{\psi}_{200} = -(i2\delta_a + \Gamma)\psi_{200} - i\sqrt{2}\Lambda^*\psi_{110} + \sqrt{2}\gamma\psi_{100}^{(2)}\xi_{in}, \quad (57a)$$

$$\begin{aligned} \dot{\psi}_{110} = & -\left(i(\delta_a + \delta_b) + \frac{\Gamma + \gamma_L}{2}\right)\psi_{110} - i\sqrt{2}\Lambda\psi_{200} \\ & - i\sqrt{2}\Lambda^*\psi_{020} + \sqrt{\gamma}\psi_{010}^{(2)}\xi_{in}, \end{aligned} \quad (57b)$$

$$\dot{\psi}_{020} = -(i2\delta_b + \gamma_L)\psi_{020} - i\sqrt{2}\Lambda\psi_{110} - i\sqrt{2}\chi_2\psi_{001}, \quad (57c)$$

$$\dot{\psi}_{001} = -\left(i\delta_c + \frac{\gamma_L}{2}\right)\psi_{001} - i\sqrt{2}\chi_2\psi_{020}. \quad (57d)$$

It is the fact that SHG requires two input photons that enables the phase condition $\Delta\vartheta = \pi$ to be fulfilled. To understand why, consider the case in which the storage time is adjusted such that a single Rabi oscillation between states $|020\rangle$ and $|001\rangle$ occur. An example is shown in Fig. 8. Occupation probabilities of the system states are found in Appendix D and plotted as a function of time in Fig. 8(a). It shows how the photons are transferred from state $|020\rangle$ to $|001\rangle$ and back via SHG. The phase of $\psi_{020}(t)$ jumps by π as its amplitude becomes zero in the middle of the storage interval [red curve in Fig. 8(b)]. The phase of $\psi_{01}(t)$ [blue curve in Fig. 8(b)] remains constant since a single photon cannot undergo SHG. The relevant phase difference, $\Delta\vartheta$, is therefore seen to be exactly π . Figure 8(c) shows the error in the output wave packet for both single- and two-photon inputs. Only a negligible error is observed for the single-photon input

whereas the two-photon error is more pronounced, leading to a fidelity of $F_2 = 99.1\%$ for this example. Similar to the case of a $\chi^{(3)}$ material, the fidelity of two-photon outputs are degraded by the photon-photon interaction occurring during the absorption and emission process, which is not accounted for in the solution of the control fields.

C. Interaction with a two-level emitter

We investigate the use of atomlike two-level emitters because their nonlinearity is much stronger than the nonresonant nonlinearities considered above. To ensure complete absorption of incoming photons, the TLE should not be coupled to mode b since we expect the nonlinear interaction during absorption and emission to be prohibitively strong. Instead, we use a tertiary mode, c , with $\omega_c - \omega_b \neq \omega_b - \omega_a$, which ensures that modes b and c are not coupled via the control field $\Lambda(t)$. We envision a control scheme where a first control pulse, $\Lambda_i(t)$, is used to absorb incoming photons into mode b . Subsequently, a second control pulse, $\Pi(t)$, couples modes b and c . Finally, a third control pulse, $\Lambda_o(t)$, couples the photons back into the waveguide through mode a . The first and last stages of this control protocol are therefore still described by the equations of motion in Sec. IV D. With the introduction of cavity mode c and the TLE, states with two photons in the system are $|100\rangle|e\rangle$, $|010\rangle|e\rangle$, $|001\rangle|e\rangle$, $|200\rangle|g\rangle$, $|020\rangle|g\rangle$, $|002\rangle|g\rangle$, $|110\rangle|g\rangle$, $|101\rangle|g\rangle$, and $|011\rangle|g\rangle$.

During the second stage of the protocol, mode a is empty so we introduce new coefficients, $\phi_{n_b n_c g}(t)$ and $\phi_{n_b n_c e}(t)$, corresponding to states $|0n_b n_c\rangle|g\rangle$ and $|0n_b n_c\rangle|e\rangle$. The dynamics is governed by the following equations of motion:

$$\dot{\phi}_{20g} = -(i2\delta_b + \gamma_L + i\chi_3 + i4|\Pi|)\phi_{20g} - i\sqrt{2}\Pi^*\phi_{11g}, \quad (58a)$$

$$\begin{aligned} \dot{\phi}_{11g} = & -[i(\delta_b + \delta_c) + \gamma_L + i\chi_3 + i4|\Pi|]\phi_{11g} \\ & - i\sqrt{2}\Pi\phi_{20g} - i\sqrt{2}\Pi^*\phi_{02g} - ig\phi_{10e}, \end{aligned} \quad (58b)$$

$$\begin{aligned} \dot{\phi}_{02g} = & -(i2\delta_c + \gamma_L + i\chi_3 + i4|\Pi|)\phi_{02g} \\ & - i\sqrt{2}\Pi\phi_{11g} - i\sqrt{2}g\phi_{01e}, \end{aligned} \quad (58c)$$

$$\begin{aligned} \dot{\phi}_{10e} = & -\left[i(\delta_b + \delta_e) + \frac{\gamma_e + \gamma_L}{2} + i2|\Pi|\right]\phi_{10e} \\ & - i\Pi^*\phi_{01e} - ig^*\phi_{11g}, \end{aligned} \quad (58d)$$

$$\begin{aligned} \dot{\phi}_{01e} = & -\left[i(\delta_c + \delta_e) + \frac{\gamma_e + \gamma_L}{2} + i2|\Pi|\right]\phi_{01e} \\ & - i\Pi\phi_{10e} - i\sqrt{2}g^*\phi_{02g}. \end{aligned} \quad (58e)$$

Note that the dynamics is also changed for single-photon inputs, which have the following equations of motion:

$$\dot{\phi}_{10g} = -\left(i\delta_b + \frac{\gamma_L}{2} + i2|\Pi|\right)\phi_{10g} - i\Pi^*\phi_{01g}, \quad (59a)$$

$$\dot{\phi}_{01g} = -\left(i\delta_c + \frac{\gamma_L}{2} + i2|\Pi|\right)\phi_{01g} - i\Pi\phi_{10g} - ig\phi_{00e}, \quad (59b)$$

$$\dot{\phi}_{00e} = -\left(i\delta_e + \frac{\gamma_e}{2}\right)\phi_{00e} - ig^*\phi_{01g}. \quad (59c)$$

Many interesting properties of the nonlinear interaction may be investigated using Eqs. (58) and (59), but here we again consider the implementation of a C-phase gate. With the protocol described above, the conditions for a successful gate operation are the following: (1) The occupation probability of

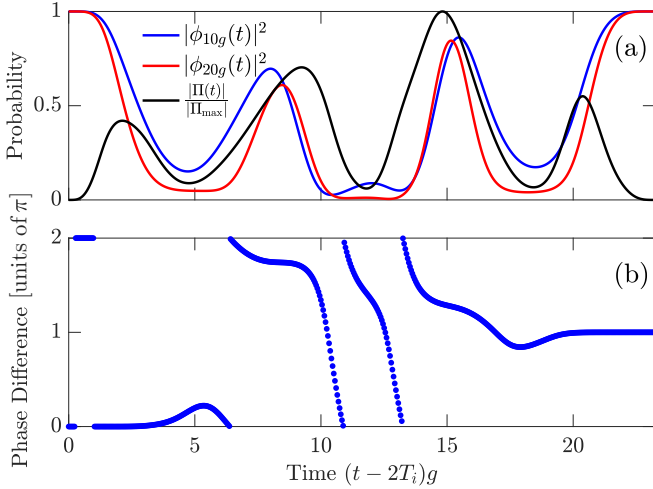


FIG. 9. Time evolution of the second stage of the control protocol. (a) Probability that all incoming photons occupy mode b for one- (blue) and two-photon (red) inputs. The control function is also plotted (scaled to a maximum of 1). (b) Phase difference $\arg[\phi_{20g}(t - 2T_i)] - 2 \arg[\phi_{10g}(t - 2T_i)]$ as a function of time. Parameters: $\gamma_L = 0$.

mode b must equal one for both single- and two-photon inputs after the application of $\Pi(t)$. (2) The phase difference must be $\arg[\phi_{20g}(T_\Pi)] - 2 \arg[\phi_{10g}(T_\Pi)] = \pi$, where $\Pi(t)$ is nonzero only in the interval $t \in [2T_i, T_\Pi]$. We numerically optimize the control function $\Pi(t)$ to fulfill these conditions. An example of the resulting dynamics is shown in Fig. 9. It shows how the conditions above may be met using a control function plotted in Fig. 9(a).

Here, we considered the host crystal containing the TLE to be a third-order nonlinear material. The optical control fields would not interact with the TLE as they would be very far off-resonant. However, it would be interesting to consider the TLE coupled to mode b and letting $\Pi(t)$ be a strong electrical field that causes a detuning between the TLE and mode b during absorption and emission via an AC Stark shift of the TLE transition energy. This would reduce the effective nonlinear coupling between the photons during absorption and emission and could potentially eliminate the need for mode c .

Note that the three-stage control protocol avoids any error due to nonlinear interactions between the photons during absorption and emission. The fidelity of a C-phase gate with a TLE nonlinearity is therefore only limited by loss when no decoherence mechanisms are included in the model. A similar extension of the control protocol could be applied to the case of second-order nonlinearities by introducing a fourth mode, b' , coupled to mode c via SHG. The second control field, $\Pi(t)$, coupling modes b and b' would then effectively turn on the nonlinearity after the photons were coupled into mode b . Alternatively, letting $\Pi(t)$ be an electric field that induces a $\chi^{(2)}$ coefficient in a material with a third-order nonlinearity [46] would constitute an equivalent method to the AC stark shift of a TLE.

VII. DISCUSSION

Our simulation results illustrate that, within the limitations of our model, it is possible to absorb and emit photons with

Gaussian wave packets into and out of a dynamically coupled cavity. We also show that high-fidelity C-phase gates may be implemented using such structures with three different types of nonlinearity. These fidelities were obtained while excluding certain sources of error from our analysis including noise photons being injected from the loss channel, decoherence of the TLE, and higher order nonlinear effects.

We analyzed the interaction with two-level emitters in the context of two-qubit gates, but we expect dynamically coupled cavities to provide performance improvements in other applications as well. For instance, perfect state transfer between photonic qubits and solid-state matter qubits has been proposed using classical control fields coupling the energy levels of the matter qubit [47]. There is a strong analogy between that method and dynamically coupled cavities; however, we expect it to be easier to engineer the photonic rather than the atomic degrees of freedom in practical implementations.

ACKNOWLEDGMENTS

The authors thank Joshua Combes and Jeffrey Shapiro for many useful discussions. This work was partly funded by the AFOSR program FA9550-16-1-0391 (D.E.), the MITRE Quantum Moonshot Program (M.H. and D.E.), the ARL DIRA ECI Grant ‘‘Photonic Circuits for Compact (Room-Temperature) Nodes for Quantum Networks’’ (K.J.), and the Velux Foundations (M.H.).

APPENDIX A: ROTATING FRAME

The Hamiltonian of the three cavity modes, four pump fields, and the TLE is \hat{H} , where

$$\begin{aligned} \frac{\hat{H}}{\hbar} = & \omega_a \hat{a}^\dagger \hat{a} + \omega_b \hat{b}^\dagger \hat{b} + \omega_c \hat{c}^\dagger \hat{c} + \omega_p \hat{p}^\dagger \hat{p} + \omega_1 \hat{p}_1^\dagger \hat{p}_1 + \omega_2 \hat{p}_2^\dagger \hat{p}_2 \\ & + \omega_3 \hat{p}_3^\dagger \hat{p}_3 + \omega_e \hat{\sigma}_z + i \sqrt{\frac{\gamma}{\Delta t}} (\hat{a}^\dagger \hat{w}_n - \hat{a} \hat{w}_n^\dagger) \\ & + \omega_w \sum_{k=1}^N \hat{w}_k^\dagger \hat{w}_k + \chi_2 (\hat{p}^\dagger \hat{a}^\dagger \hat{b} + \hat{p} \hat{b}^\dagger \hat{a}) + \chi_3 (\hat{p}_1^\dagger \hat{p}_2 \hat{a}^\dagger \hat{b} \\ & + \hat{p}_2^\dagger \hat{p}_1 \hat{b}^\dagger \hat{a}) + \chi_3 (\hat{p}_1^\dagger \hat{p}_3 \hat{b}^\dagger \hat{c} + \hat{p}_3^\dagger \hat{p}_1 \hat{c}^\dagger \hat{b}). \end{aligned} \quad (\text{A1})$$

(Since we wish merely to provide an example, we have left out the cross-phase modulation, self-phase modulation, and second-order harmonic generation from the Hamiltonian.) We wish to move into the interaction picture, placing the evolution generated by the Hamiltonian \hat{H}_0 into the operators, where

$$\begin{aligned} \frac{\hat{H}_0}{\hbar} = & \omega_w \hat{a}^\dagger \hat{a} + (\omega_b - \delta_b) \hat{b}^\dagger \hat{b} + (\omega_c - \delta_c) \hat{c}^\dagger \hat{c} + \omega_e \hat{\sigma}_z \\ & + \omega_p \hat{p}^\dagger \hat{p} + \omega_1 \hat{p}_1^\dagger \hat{p}_1 + \omega_2 \hat{p}_2^\dagger \hat{p}_2 + \omega_3 \hat{p}_3^\dagger \hat{p}_3 \\ & + \omega_w \sum_{k=1}^N \hat{w}_k^\dagger \hat{w}_k. \end{aligned} \quad (\text{A2})$$

Under this Hamiltonian, the evolution of the operators is obtained merely by multiplying them by time-dependent exponentials. Denoting the interaction-picture operators by upper-case letters, we have $\hat{A} = \hat{a} e^{-i\omega_w t}$, $\hat{B} = \hat{b} e^{-i(\omega_b - \delta_b)t}$, $\hat{C} = \hat{c} e^{-i(\omega_c - \delta_c)t}$, $\hat{\Sigma}_z = \hat{\sigma}_z e^{-i\omega_e t}$, $\hat{P} = \hat{p} e^{-i\omega_p t}$, $\hat{P}_j = \hat{p}_j e^{-i\omega_j t}$ ($j =$

1, 2, 3), $\hat{W}_k = \hat{w}_k e^{-i\omega_w t}$. Since we have removed this “rotating” evolution from the state of the system, we refer to the interaction picture as being in a “rotating frame.”

The evolution of the state of the system is now given by an effective interaction Hamiltonian, usually referred to as the “interaction Hamiltonian in the interaction picture,” which is given by

$$\hat{H}_1(t) = \hat{U}(\hat{H} - \hat{H}_0)\hat{U}^\dagger \quad (\text{A3})$$

in which $\hat{U} = e^{-i\hat{H}_0 t/\hbar}$. Since the right-hand side of the above equation is merely the Hamiltonian $\hat{H} - \hat{H}_0$ evolved in the interaction picture, we obtain $\hat{H}_1(t)$ merely by replacing the Schrödinger picture operators in $\hat{H} - \hat{H}_0$ with their interaction picture counterparts given above. While in general $\hat{H}_1(t)$ will be time dependent, if we choose the detuning parameters, δ_a through δ_e , to account for the detunings between the various modes and the TLE, we obtain a time-independent interaction picture Hamiltonian, namely

$$\begin{aligned} \hat{H}_{\text{rot}} = & \hbar\delta_a \hat{a}^\dagger \hat{a} + \hbar\delta_b \hat{b}^\dagger \hat{b} + \hbar\delta_c \hat{c}^\dagger \hat{c} + \hbar\delta_e \hat{\sigma}_z \\ & + i\hbar\sqrt{\frac{\gamma}{\Delta t}}(\hat{a}^\dagger \hat{w}_n - \hat{a} \hat{w}_n^\dagger) + \hbar\chi_2(\hat{p}^\dagger \hat{a}^\dagger \hat{b} + \hat{p} \hat{b}^\dagger \hat{a}) \\ & + \hbar\chi_3(\hat{p}_1^\dagger \hat{p}_2 \hat{a}^\dagger \hat{b} + \hat{p}_2^\dagger \hat{p}_1 \hat{b}^\dagger \hat{a}) + \hbar\chi_3(\hat{p}_1^\dagger \hat{p}_3 \hat{b}^\dagger \hat{c} \\ & + \hat{p}_3^\dagger \hat{p}_1 \hat{c}^\dagger \hat{b}). \end{aligned} \quad (\text{A4})$$

For the scenario in which the nonlinearity is provided by the TLE, the various detunings are chosen to satisfy

$$\left. \begin{aligned} \delta_a &\equiv \omega_a - \omega_w \\ \delta_b &\equiv \delta_\Lambda + \delta_a \\ \delta_c &\equiv \delta_\Pi + \delta_b \\ \delta_e &\equiv \omega_e - \omega_c \\ \delta_\Lambda &\equiv (\omega_2 - \omega_1) - (\omega_a - \omega_b) \\ \delta_\Pi &\equiv (\omega_3 - \omega_1) - (\omega_b - \omega_c) \end{aligned} \right\} \text{TLE nonlinearity.} \quad (\text{A5})$$

Here we have chosen δ_b to remove the oscillating exponential factor in the FWM term corresponding to the control field $\Lambda(t)$:

$$\begin{aligned} \hat{P}_2^\dagger \hat{P}_1 \hat{B}^\dagger \hat{A} &= \hat{p}_2^\dagger \hat{p}_1 \hat{b}^\dagger \hat{a} \exp[(\omega_2 - \omega_1) + \omega_b \\ &\quad - \delta_b - (\omega_a - \delta_a)] \\ &\Rightarrow \delta_b = (\omega_2 - \omega_1) - (\omega_a - \omega_b) + \delta_a \\ &\equiv \delta_\Lambda + \delta_a, \end{aligned} \quad (\text{A6})$$

where we have defined δ_Λ , which describes energy mismatch in the FWM process that couples modes a and b . Similarly, we choose δ_c to remove any exponential factor on the FWM term corresponding to the control field $\Pi(t)$

$$\begin{aligned} \hat{P}_3^\dagger \hat{P}_1 \hat{C}^\dagger \hat{B} &= \hat{p}_3^\dagger \hat{p}_1 \hat{c}^\dagger \hat{b} \exp[(\omega_3 - \omega_1) - (\omega_b - \delta_b) \\ &\quad + (\omega_c - \delta_c)] \\ &\Rightarrow \delta_c = (\omega_3 - \omega_1) - (\omega_b - \omega_c) + \delta_b \\ &\equiv \delta_\Pi + \delta_b, \end{aligned} \quad (\text{A7})$$

where we defined δ_Π , which describes energy mismatch in the FWM process that couples modes b and c .

In a $\chi^{(2)}$ material, where there is no control field $\Pi(t)$, we instead define the detunings as

$$\left. \begin{aligned} \delta_a &\equiv \omega_a - \omega_w \\ \delta_b &\equiv \delta_\Lambda + \delta_a \\ \delta_c &\equiv \omega_c - 2\omega_b \\ \delta_\Lambda &\equiv \omega_p - (\omega_b - \omega_a) \end{aligned} \right\} \chi^{(2)} \text{ material,} \quad (\text{A8})$$

where δ_c now describes energy mismatch in the second-order harmonic generation process.

APPENDIX B: DYNAMICS WITH ONE CAVITY MODE AND ONE INPUT PHOTON

Before the dynamics begins, the state is

$$|\psi_0\rangle = \sum_{k=1}^N \xi_k^{\text{in}} \sqrt{\Delta t} |0\rangle |1_k\rangle, \quad (\text{B1})$$

where $|0\rangle |1_k\rangle$ is the state with one photon in bin k and no photons in the system. The state after each time step is found using the time evolution operator

$$|\psi_{n+1}\rangle = \hat{U}_{n+1} |\psi_n\rangle. \quad (\text{B2})$$

After the first time step, the state is therefore

$$\begin{aligned} |\psi_1\rangle = & \sum_{k=2}^N \xi_k^{\text{in}} \sqrt{\Delta t} |0\rangle |1_k\rangle + \xi_1^{\text{in}} \sqrt{\Delta t} |0\rangle |\mathbf{1}_1\rangle \\ & + \sqrt{\gamma} \xi_1^{\text{in}} \Delta t |1\rangle |\emptyset\rangle. \end{aligned} \quad (\text{B3})$$

We define the Schrödinger coefficient corresponding to the photon being in the cavity mode as $\psi_1(1) = \sqrt{\gamma} \xi_1^{\text{in}} \Delta t$. Note that we split the summation over k into input states, $n > k$, and output states, $k \leq n$, for which we use boldface notation. After the second step, the state is

$$\begin{aligned} |\psi_2\rangle = & \sum_{k=3}^N \xi_k^{\text{in}} \sqrt{\Delta t} |0\rangle |1_k\rangle + \sum_{k=1}^2 \xi_k^{\text{in}} \sqrt{\Delta t} |0\rangle |\mathbf{1}_k\rangle \\ & - \sqrt{\gamma} \psi_1(1) \sqrt{\Delta t} |0\rangle |\mathbf{1}_2\rangle \\ & + \left[\left(1 - i\delta_a \Delta t - \frac{\Gamma}{2} \Delta t\right) \psi_1(1) + \sqrt{\gamma} \xi_2^{\text{in}} \Delta t \right] |1\rangle |\emptyset\rangle, \end{aligned} \quad (\text{B4})$$

where the third term corresponds to a photon being emitted by the cavity into bin 2 on the output side. The fourth term contains a contribution from the identity operator, a detuning term, a decay term, as well as a feeding term corresponding to absorption of a photon from the waveguide in bin 2. Rewriting Eq. (B4) as

$$\begin{aligned} |\psi_2\rangle = & \sum_{k=3}^N \xi_k^{\text{in}} \sqrt{\Delta t} |0\rangle |1_k\rangle + \xi_1^{\text{out}} \sqrt{\Delta t} |0\rangle |\mathbf{1}_1\rangle \\ & + \left[\xi_2^{\text{in}} - \sqrt{\gamma} \psi_1(1) \right] \sqrt{\Delta t} |0\rangle |\mathbf{1}_2\rangle + \psi_1(2) |1\rangle |\emptyset\rangle \end{aligned} \quad (\text{B5})$$

lets us identify the update rules

$$\psi_1(n+1) = \psi_1(n) + \left[\left(-i\delta_a - \frac{\Gamma}{2} \right) \psi_1(n) + \sqrt{\gamma} \xi_{n+1}^{\text{in}} \right] \Delta t \quad (\text{B6})$$

$$\Rightarrow \frac{\psi_1(n+1) - \psi_1(n)}{\Delta t} = - \left(i\delta_a + \frac{\Gamma}{2} \right) \psi_1(n) + \sqrt{\gamma} \xi_{n+1}^{\text{in}}, \quad (\text{B7})$$

$$\xi_n^{\text{out}} = \xi_n^{\text{in}} - \sqrt{\gamma} \psi_1(n-1). \quad (\text{B8})$$

We may now take the continuum limit, $\Delta t \rightarrow 0$, to obtain the equation of motion and input-output relation

$$\dot{\psi}_1(t) = \left(-i\delta_a - \frac{\Gamma}{2} \right) \psi_1(t) + \sqrt{\gamma} \xi_{\text{in}}(t), \quad (\text{B9a})$$

$$\xi_{\text{out}}(t) = \xi_{\text{in}}(t) - \sqrt{\gamma} \psi_1(t). \quad (\text{B9b})$$

Note that we used $\psi_1(n-1) \rightarrow \psi_1(n)$ and $\xi_{n+1}^{\text{in}} \rightarrow \xi_n^{\text{in}}$ in the continuum limit, so all functions are evaluated at the same time in Eq. (B9).

APPENDIX C: DYNAMICS WITH TWO CAVITY MODES AND ONE INPUT PHOTON

Before the dynamics begins, the state is

$$|\psi_0\rangle = \sum_{k=1}^N \xi_k^{\text{in}} \sqrt{\Delta t} |00\rangle |1_k\rangle, \quad (\text{C1})$$

where $|00\rangle$ is the state with no photons in either mode a or b . After step 1, the state is

$$|\psi_1\rangle = |\psi_0\rangle + \sqrt{\gamma} \xi_1^{\text{in}} \Delta t |10\rangle |\emptyset\rangle \equiv |\psi_0\rangle + \psi_{10}(1) |10\rangle |\emptyset\rangle, \quad (\text{C2})$$

where we defined the amplitude for the state with one photon in mode a and no photons in mode b , ψ_{10} . After step 2, the state is

$$\begin{aligned} |\psi_2\rangle &= \sum_{k=3}^N \xi_k^{\text{in}} \sqrt{\Delta t} |00\rangle |1_k\rangle - \sqrt{\gamma} \psi_{10}(1) \sqrt{\Delta t} |00\rangle |\mathbf{1}_1\rangle + [\xi_2^{\text{in}} - \sqrt{\gamma} \psi_{10}(1)] \sqrt{\Delta t} |00\rangle |\mathbf{1}_2\rangle \\ &+ \left[\left(1 - i\delta_a \Delta t - \frac{\Gamma}{2} \Delta t - i2|\Lambda_2| \Delta t \right) \psi_{10}(1) + \sqrt{\gamma} \xi_2^{\text{in}} \Delta t \right] |10\rangle |\emptyset\rangle - i\Lambda_2 \psi_{10}(1) \Delta t |01\rangle |\emptyset\rangle \\ &\equiv \sum_{k=3}^N \xi_k^{\text{in}} \sqrt{\Delta t} |00\rangle |1_k\rangle + \sum_{k=1}^2 \xi_k^{\text{out}} \sqrt{\Delta t} |00\rangle |\mathbf{1}_k\rangle + \psi_{10}(1) |10\rangle |\emptyset\rangle + \psi_{01}(1) |01\rangle |\emptyset\rangle. \end{aligned} \quad (\text{C3})$$

After step 3, the state is

$$\begin{aligned} |\psi_3\rangle &= \sum_{k=4}^N \xi_k^{\text{in}} \sqrt{\Delta t} |00\rangle |1_k\rangle + \sum_{k=1}^3 \xi_k^{\text{out}} \sqrt{\Delta t} |00\rangle |\mathbf{1}_k\rangle + \left[\left(1 - i\delta_b \Delta t - \frac{\gamma L}{2} \Delta t - i2|\Lambda_3| \Delta t \right) \psi_{01}(2) \right. \\ &\left. - i\Lambda_3 \psi_{10}(2) \Delta t \right] |01\rangle |\emptyset\rangle + \left[\left(1 - i\delta_a \Delta t - \frac{\Gamma}{2} \Delta t - i2|\Lambda_3| \Delta t \right) \psi_{10}(2) - i\Lambda_3^* \psi_{01}(2) \Delta t + \sqrt{\gamma} \xi_3^{\text{in}} \Delta t \right] |10\rangle |\emptyset\rangle. \end{aligned} \quad (\text{C4})$$

Equation (C4) contains all the possible dynamics and we can use it to read off the update rules:

$$\frac{\psi_{10}(n+1) - \psi_{10}(n)}{\Delta t} = \left(-i\delta_a - \frac{\Gamma}{2} - i2|\Lambda_{n+1}| \right) \psi_{10}(n) - i\Lambda_{n+1}^* \psi_{01}(n) + \sqrt{\gamma} \xi_{n+1}^{\text{in}}, \quad (\text{C5})$$

$$\frac{\psi_{01}(n+1) - \psi_{01}(n)}{\Delta t} = \left(-i\delta_b - \frac{\gamma L}{2} - i2|\Lambda_{n+1}| \right) \psi_{01}(n) - i\Lambda_{n+1} \psi_{10}(n), \quad (\text{C6})$$

$$\xi_n^{\text{out}} = \xi_n^{\text{in}} - \sqrt{\gamma} \psi_{10}(n-1). \quad (\text{C7})$$

In the continuum limit, we have the ODEs and input-output relation

$$\dot{\psi}_{10}(t) = - \left(i\delta_a + \frac{\Gamma}{2} + i2|\Lambda(t)| \right) \psi_{10}(t) - i\Lambda(t)^* \psi_{01}(t) + \sqrt{\gamma} \xi_{\text{in}}(t), \quad (\text{C8a})$$

$$\dot{\psi}_{01}(t) = - \left(i\delta_b + \frac{\gamma L}{2} + i2|\Lambda(t)| \right) \psi_{01}(t) - i\Lambda(t) \psi_{10}(t), \quad (\text{C8b})$$

$$\xi_{\text{out}}(t) = \xi_{\text{in}}(t) - \sqrt{\gamma} \psi_{10}(t). \quad (\text{C8c})$$

APPENDIX D: DYNAMICS WITH TWO CAVITY MODES AND TWO INPUT PHOTONS

For identical input photons, the input state is

$$|\psi_0\rangle = \sqrt{2} \sum_{j=1}^N \sum_{k>j}^N \xi_j^{\text{in}} \xi_k^{\text{in}} \Delta t |00\rangle |1_j 1_k\rangle. \quad (\text{D1})$$

Let us show that the state in Eq. (D1) is normalized. In the continuum limit, it corresponds to

$$|\psi\rangle = \sqrt{2} \int_{t_0}^{t_N} dt_j \int_{t_j}^{t_N} dt_k \xi(t_j) \xi(t_k) |00\rangle |1_j 1_k\rangle, \quad (\text{D2})$$

where we omitted the *in* superscripts. Let us calculate its norm

$$\langle\psi|\psi\rangle = 2 \int_{t_0}^{t_N} dt'_j \int_{t'_j}^T dt'_k \int_{t_0}^{t_N} dt_j \int_{t_j}^{t_N} dt_k \xi^*(t'_j) \xi(t_j) \xi^*(t'_k) \xi(t_k) \langle 1'_j | 1_j \rangle \langle 1'_k | 1_k \rangle \quad (\text{D3a})$$

$$\Rightarrow \langle\psi|\psi\rangle = 2 \int_{t_0}^{t_N} dt_j |\xi(t_j)|^2 \int_{t_j}^{t_N} dt_k |\xi(t_k)|^2 = 2 \int_{t_0}^{t_N} dt_j |\xi(t_j)|^2 \left[\int_{t_0}^{t_N} dt_k |\xi(t_k)|^2 - \int_{t_0}^{t_j} dt_k |\xi(t_k)|^2 \right] \quad (\text{D3b})$$

$$\Rightarrow \langle\psi|\psi\rangle = 2 \int_{t_0}^{t_N} dt_j |\xi(t_j)|^2 \left[1 - \int_{t_0}^{t_j} dt_k |\xi(t_k)|^2 \right] = 2 - 2 \int_{t_0}^{t_N} dt_j |\xi(t_j)|^2 \int_{t_0}^{t_j} dt_k |\xi(t_k)|^2 \quad (\text{D3c})$$

$$\Rightarrow \langle\psi|\psi\rangle = 2 - 2 \int_{t_0}^{t_N} dt_j \dot{\Xi}(t_j) \Xi(t_j) = 2 - 2 \int_{t_0}^{t_N} dt_j \frac{d}{dt_j} \left(\frac{1}{2} \Xi^2(t_j) \right) = 2 - [\Xi(T) - \Xi(0)] = 2 - (1 - 0) = 1, \quad (\text{D3d})$$

where $\dot{\Xi}(t_j) = |\xi(t_j)|^2$.

To begin with, we follow the dynamics of states with one photon in the system and one photon on the input side,

$$|\psi_n\rangle = \psi_{10}^{(2)}(n) \sum_{k>n}^N \xi_k^{\text{in}} \sqrt{\Delta t} |10\rangle |1_k\rangle + \psi_{01}^{(2)}(n) \sum_{k>n}^N \xi_k^{\text{in}} \sqrt{\Delta t} |01\rangle |1_k\rangle + \dots \quad (\text{D4})$$

The superscript “(2)” signifies that the equation of motion for $\psi_{10}^{(2)}(t)$ is driven by two photons in the input side. As in Appendixes B and C, we follow the evolution of these states through the first time steps in order to identify the update rules. After the first step, we have

$$|\psi_1\rangle = \sqrt{2} \xi_1^{\text{in}} \sqrt{\gamma} \Delta t \sum_{k>1}^N \xi_k^{\text{in}} \sqrt{\Delta t} |10\rangle |1_k\rangle + \dots = \psi_{10}^{(2)}(1) \sum_{k>1}^N \xi_k^{\text{in}} \sqrt{\Delta t} |10\rangle |1_k\rangle + \dots, \quad (\text{D5})$$

After step 2, we have

$$\begin{aligned} |\psi_2\rangle &= \left[\left(1 - i\delta_a \Delta t - \frac{\Gamma}{2} \Delta t - i2|\Lambda_2| \Delta t \right) \psi_{10}^{(2)}(1) + \sqrt{2} \xi_2^{\text{in}} \sqrt{\gamma} \Delta t \right] \sum_{k>2}^N \xi_k^{\text{in}} \sqrt{\Delta t} |10\rangle |1_k\rangle - i\Lambda_2 \psi_{10}^{(2)}(1) \sum_{k>2}^N \xi_k^{\text{in}} \sqrt{\Delta t} |01\rangle |1_k\rangle + \dots \\ &= \psi_{10}^{(2)}(2) \sum_{k>2}^N \xi_k^{\text{in}} \sqrt{\Delta t} |10\rangle |1_k\rangle + \psi_{01}^{(2)}(2) \sum_{k>2}^N \xi_k^{\text{in}} \sqrt{\Delta t} |01\rangle |1_k\rangle + \dots \end{aligned} \quad (\text{D6})$$

After step 3, all the possible interactions linking $\psi_{10}^{(2)}$ and $\psi_{01}^{(2)}$ are included:

$$\begin{aligned} |\psi_3\rangle &= \left[\left(1 - i\delta_a \Delta t - \frac{\Gamma}{2} \Delta t - i2|\Lambda_3| \Delta t \right) \psi_{10}^{(2)}(2) + \sqrt{2} \xi_3^{\text{in}} \sqrt{\gamma} \Delta t - i\Lambda_3^* \psi_{01}^{(2)}(2) \Delta t \right] \sum_{k>3}^N \xi_k^{\text{in}} \sqrt{\Delta t} |10\rangle |1_k\rangle \\ &+ \left[\left(1 - i\delta_b \Delta t - \frac{\gamma L}{2} \Delta t - i2|\Lambda_3| \Delta t \right) \psi_{01}^{(2)}(2) - i\Lambda_3 \psi_{10}^{(2)}(2) \Delta t \right] \sum_{k>3}^N \xi_k^{\text{in}} \sqrt{\Delta t} |01\rangle |1_k\rangle + \dots \end{aligned} \quad (\text{D7})$$

From Eq. (D7), we identify the equations of motion in the continuum limit

$$\dot{\psi}_{10}^{(2)}(t) = - \left(i\delta_a - \frac{\Gamma}{2} + i2|\Lambda(t)| \right) \psi_{10}^{(2)}(t) - i\Lambda(t)^* \psi_{01}^{(2)}(t) + \sqrt{2\gamma} \xi_{\text{in}}(t), \quad (\text{D8a})$$

$$\dot{\psi}_{01}^{(2)}(t) = - \left(i\delta_b - \frac{\gamma L}{2} + i2|\Lambda(t)| \right) \psi_{01}^{(2)}(t) - i\Lambda(t) \psi_{10}^{(2)}(t). \quad (\text{D8b})$$

Next, we consider states with two photons in the system

$$|\psi_n\rangle = \psi_{20}(n)|20\rangle|\emptyset\rangle + \psi_{11}(n)|11\rangle|\emptyset\rangle + \psi_{02}(n)|02\rangle|\emptyset\rangle + \dots \quad (\text{D9})$$

These states first appear after step 2:

$$|\psi_2\rangle = \sqrt{2\gamma}\psi_{10}^{(2)}(1)\xi_2^{\text{in}}\Delta t|20\rangle|\emptyset\rangle + \sqrt{\gamma}\psi_{01}^{(2)}(1)\xi_2^{\text{in}}\Delta t|11\rangle|\emptyset\rangle + \dots = \psi_{20}(2)|20\rangle|\emptyset\rangle + \psi_{11}(2)|11\rangle|\emptyset\rangle + \dots, \quad (\text{D10})$$

where the factor of $\sqrt{2}$ in the first term comes from \hat{a}^\dagger acting on $|10\rangle$. After step 3, we have

$$\begin{aligned} |\psi_3\rangle = & \left[(1 - i2\delta_a\Delta t - \Gamma\Delta t - i4|\Lambda_3|\Delta t)\psi_{20}(2) - i\sqrt{2}\Lambda_3^*\psi_{11}(2)\Delta t + \psi_{10}^{(2)}(2)\xi_3^{\text{in}}\sqrt{2\gamma}\Delta t \right] |20\rangle|\emptyset\rangle \\ & + \left[\left(1 - i(\delta_a + \delta_b)\Delta t - \frac{\Gamma + \gamma_L}{2}\Delta t - i4|\Lambda_3|\Delta t \right) \psi_{11}(2) - i\sqrt{2}\Delta t\Lambda_3\psi_{20}(2) + \sqrt{\gamma}\psi_{01}^{(2)}(2)\xi_3^{\text{in}}\Delta t \right] |11\rangle|\emptyset\rangle \\ & - i\sqrt{2}\Lambda_3\psi_{11}(2)\Delta t|02\rangle|\emptyset\rangle + \dots \end{aligned} \quad (\text{D11})$$

After step 4, all the dynamics describing the states with two photons in the system is present

$$\begin{aligned} |\psi_4\rangle = & \left[(1 - i2\delta_a\Delta t - \Gamma\Delta t - i4|\Lambda_4|\Delta t)\psi_{20}(3) - i\sqrt{2}\Lambda_4^*\psi_{11}(3)\Delta t + \psi_{10}^{(2)}(3)\xi_4^{\text{in}}\sqrt{2\gamma}\Delta t \right] |20\rangle|\emptyset\rangle \\ & + \left[\left(1 - i(\delta_a + \delta_b)\Delta t + \frac{\Gamma + \gamma_L}{2}\Delta t - i4|\Lambda_4|\Delta t \right) \psi_{11}(3) - i\sqrt{2}\Delta t(\Lambda_4\psi_{20}(3) + \Lambda_4^*\psi_{02}(3)) + \psi_{01}^{(2)}(3)\xi_4^{\text{in}}\sqrt{\gamma}\Delta t \right] |11\rangle|\emptyset\rangle \\ & + [(1 - i2\delta_b - \gamma_L\Delta t - i4|\Lambda_4|\Delta t)\psi_{02}(3) - i\sqrt{2}\Lambda_4\psi_{11}(3)]|02\rangle|\emptyset\rangle + \dots \end{aligned} \quad (\text{D12})$$

We identify the equations of motion in the continuum limit

$$\dot{\psi}_{20}(t) = -(i2\delta_a + \Gamma + i4|\Lambda(t)|)\psi_{20}(t) - i\sqrt{2}\Lambda(t)^*\psi_{11}(t) + \sqrt{2\gamma}\psi_{10}^{(2)}(t)\xi_{\text{in}}(t), \quad (\text{D13a})$$

$$\dot{\psi}_{11}(t) = -\left(i(\delta_a + \delta_b) + \frac{\Gamma + \gamma_L}{2} + i4|\Lambda(t)|\right)\psi_{11}(t) - i\sqrt{2}\Lambda(t)\psi_{20}(t) - i\sqrt{2}\Lambda(t)^*\psi_{02}(t) + \sqrt{\gamma}\psi_{01}^{(2)}(t)\xi_{\text{in}}(t), \quad (\text{D13b})$$

$$\dot{\psi}_{02}(t) = -(i2\delta_b + \gamma_L + i4|\Lambda(t)|)\psi_{02}(t) - i\sqrt{2}\Lambda(t)\psi_{11}(t). \quad (\text{D13c})$$

Next, we consider states with one photon on the input side and one on the output side. There are two paths resulting in this state (see Fig. 3). (1) A photon is emitted into the waveguide from the system while the other photon remains on the input side. (2) One of the two input photons passes by the system without interacting. If this occurs in bin m , the contribution to the state is

$$|\psi_m\rangle = [-\sqrt{\gamma}\psi_{10}^{(2)}(m) + \sqrt{2}\xi_m^{\text{in}}] \sum_{k>m}^N \xi_k^{\text{in}}\Delta t|00\rangle|1_k\mathbf{1}_m\rangle + \dots = \psi_{00}(m) \sum_{k>m}^N \xi_k^{\text{in}}\Delta t|00\rangle|1_k\mathbf{1}_m\rangle + \dots \quad (\text{D14})$$

If the photon remaining on the input side is absorbed, it gives rise to states with one photon in the system and one on the output side

$$|\psi_n\rangle = \psi_{00}(m)[\psi_{10}^{(1)}(m, n)\sqrt{\Delta t}|10\rangle|\mathbf{1}_m\rangle + \psi_{01}^{(1)}(m, n)\sqrt{\Delta t}|01\rangle|\mathbf{1}_m\rangle] + \dots, \quad (\text{D15})$$

where we factored out $\psi_{00}(m)$ to obtain equations of motion for $\psi_{10}^{(1)}(t_m, t)$ and $\psi_{01}^{(1)}(t_m, t)$ that are similar to Eq. (D8). These amplitudes are functions of two times, where t_m describes the time the dynamics was initialized by the formation of the state $|1_k\mathbf{1}_m\rangle$. The superscript “(1)” signifies that the equations of motion for $\psi_{10}^{(1)}(t_m, t)$ and $\psi_{01}^{(1)}(t_m, t)$ are driven by one photon on the input side. Let us again follow the evolution of Eq. (D15) for a few time steps to determine the equations of motion for $\psi_{10}^{(1)}(t_m, t)$ and $\psi_{01}^{(1)}(t_m, t)$. At step $n + 1$, we have

$$\begin{aligned} \frac{|\psi_{n+1}\rangle}{\psi_{00}(m)} = & \left[\left(1 - i\delta_a\Delta t - \frac{\Gamma}{2}\Delta t - i2|\Lambda_{n+1}|\Delta t \right) \psi_{10}^{(1)}(m, n) - i\Lambda_{n+1}^*\psi_{01}(m, n)\Delta t + \sqrt{\gamma}\xi_{n+1}^{\text{in}}\Delta t \right] \sqrt{\Delta t}|10\rangle|\mathbf{1}_m\rangle \\ & + \left[\left(1 - i\delta_b\Delta t - \frac{\gamma_L}{2}\Delta t - i2|\Lambda_{n+1}|\Delta t \right) \psi_{01}^{(1)}(m, n) - i\Lambda_{n+1}\psi_{10}(m, n)\Delta t \right] \sqrt{\Delta t}|01\rangle|\mathbf{1}_m\rangle + \dots \\ = & \psi_{10}^{(1)}(m, n+1)\sqrt{\Delta t}|10\rangle|\mathbf{1}_m\rangle + \psi_{01}^{(1)}(m, n+1)\sqrt{\Delta t}|01\rangle|\mathbf{1}_m\rangle + \dots \end{aligned} \quad (\text{D16})$$

From Eq. (D16), we obtain the equations of motion

$$\dot{\psi}_{10}^{(1)}(t_m, t) = -\left(i\delta_a + \frac{\Gamma}{2} + i2|\Lambda(t)|\right)\psi_{10}^{(1)}(t_m, t) - i\Lambda(t)^*\psi_{01}^{(1)}(t_m, t) + \sqrt{\gamma}\xi_{\text{in}}(t), \quad (\text{D17a})$$

$$\dot{\psi}_{01}^{(1)}(t_m, t) = -\left(i\delta_b + \frac{\gamma_L}{2} + i2|\Lambda(t)|\right)\psi_{01}^{(1)}(t_m, t) - i\Lambda(t)\psi_{10}^{(1)}(t_m, t). \quad (\text{D17b})$$

Comparing Eqs. (D8) and (D17), we see that there is an additional factor of $\sqrt{2}$ on the driving term $\sqrt{\gamma}\xi_{\text{in}}(t)$ in Eq. (D8) because it is driven by two photons as opposed to one in Eq. (D17). The initial condition for Eq. (D17) is $\psi_{10}^{(1)}(t_m, t_m)=0$ and $\psi_{01}^{(1)}(t_m, t_m)=0$ because the system started out in the state $|00\rangle$ in Eq. (D14).

Finally, we need to consider states with one photon in the system and one photon on the output side

$$|\psi_n\rangle = \psi_{10}^{(0)}(m, n)\sqrt{\Delta t}|10\rangle|\mathbf{1}_m\rangle + \psi_{01}^{(0)}(m, n)\sqrt{\Delta t}|01\rangle|\mathbf{1}_m\rangle + \dots, \quad (\text{D18})$$

There are four different paths leading to this state. One (two), a photon is emitted into the waveguide while the state of the system is $|20\rangle$ ($|11\rangle$). Three (four), the photon on the input side passes by the system without interacting while the system is in the state $|10\rangle$ ($|01\rangle$). If this occurs in bin m , the contribution to the state is

$$\begin{aligned} |\psi_m\rangle &= [-\sqrt{2\gamma}\psi_{20}(m) + \psi_{10}^{(2)}(m)\xi_m^{\text{in}}]\sqrt{\Delta t}|10\rangle|\mathbf{1}_m\rangle + [-\sqrt{\gamma}\psi_{11}(m) + \psi_{01}^{(2)}(m)\xi_m^{\text{in}}]\sqrt{\Delta t}|01\rangle|\mathbf{1}_m\rangle + \dots \\ &= \psi_{10}^{(0)}(m, m)\sqrt{\Delta t}|10\rangle|\mathbf{1}_m\rangle + \psi_{01}^{(0)}(m, m)\sqrt{\Delta t}|01\rangle|\mathbf{1}_m\rangle + \dots \end{aligned} \quad (\text{D19})$$

At time t_{m+1} , the state is

$$\begin{aligned} |\psi_{m+1}\rangle &= \left[\left(1 - i\delta_a\Delta t - \frac{\Gamma}{2}\Delta t - i2|\Lambda_{m+1}|\Delta t \right) \psi_{10}^{(0)}(m, m) - i\Lambda_{m+1}^* \psi_{01}^{(0)}(m, m)\Delta t \right] \sqrt{\gamma\Delta t}|10\rangle|\mathbf{1}_m\rangle \\ &\quad + \left[\left(1 - i\delta_b\Delta t - \frac{\gamma L}{2}\Delta t - i2|\Lambda_{m+1}|\Delta t \right) \psi_{01}^{(0)}(m, m) - i\Lambda_{m+1} \psi_{10}^{(0)}(m, m)\Delta t \right] \sqrt{\gamma\Delta t}|01\rangle|\mathbf{1}_m\rangle + \dots \\ &= \psi_{10}^{(0)}(m, m+1)\sqrt{\Delta t}|10\rangle|\mathbf{1}_m\rangle + \psi_{01}^{(0)}(m, m+1)\sqrt{\Delta t}|01\rangle|\mathbf{1}_m\rangle + \dots \end{aligned} \quad (\text{D20})$$

From Eq. (D20), we identify the equations of motion

$$\dot{\psi}_{10}^{(0)}(t_m, t) = -\left(i\delta_a + \frac{\Gamma}{2} + i2|\Lambda(t)| \right) \psi_{10}^{(0)}(t_m, t) - i\Lambda(t)^* \psi_{01}^{(0)}(t_m, t), \quad (\text{D21a})$$

$$\dot{\psi}_{01}^{(0)}(t_m, t) = -\left(i\delta_b + \frac{\gamma L}{2} + i2|\Lambda(t)| \right) \psi_{01}^{(0)}(t_m, t) - i\Lambda(t) \psi_{10}^{(0)}(t_m, t). \quad (\text{D21b})$$

Equation (D21) must be solved for two sets of initial conditions corresponding to the first [$\psi_{10}^{(0)}(t_m, t_m)=1$ and $\psi_{01}^{(0)}(t_m, t_m)=0$] and second [$\psi_{10}^{(0)}(t_m, t_m)=0$ and $\psi_{01}^{(0)}(t_m, t_m)=1$] term in Eq. (D18), respectively. We introduce functions $A_{10}(t_m, t)$, $A_{01}(t_m, t)$, $B_{10}(t_m, t)$, and $B_{01}(t_m, t)$, where A correspond to $\psi^{(0)}$ with the first initial condition and B correspond to $\psi^{(0)}$ with the second initial condition.

The final step is to identify all terms of the output state using Fig. 3 and the derivations above. From Eq. (D14), we have the contributions

$$\xi_{\text{out}}(t_m, t) = -\sqrt{\gamma}\psi_{10}^{(1)}(t_m, t)[- \sqrt{\gamma}\psi_{10}^{(2)}(t_m) + \sqrt{2}\xi_{\text{in}}(t_m)] + \dots, \quad (\text{D22})$$

where the first factor is the probability amplitude for decay from state $|10\rangle$ into the waveguide at time t , and the terms in brackets are the two contributions to the probability amplitude of a photon entering the waveguide at time t_m . From Eq. (D19), we have the contributions

$$\xi_{\text{out}}(t_m, t) = -\sqrt{\gamma}A_{10}(t_m, t)[- \sqrt{2\gamma}\psi_{20}(t_m) + \psi_{10}^{(2)}(t_m)\xi_{\text{in}}(t_m)] - \sqrt{\gamma}B_{10}(t_m, t)[- \sqrt{\gamma}\psi_{11}(t_m) + \psi_{01}^{(2)}(t_m)\xi_{\text{in}}(t_m)] + \dots. \quad (\text{D23})$$

The remaining contributions to the output state come from both photons passing by the system without interacting and decay from system state $|10\rangle$ followed by the second input photon passing by the system

$$\xi_{\text{out}}(t_m, t) = [\sqrt{2}\xi_{\text{in}}(t_m) - \sqrt{\gamma}\psi_{10}^{(2)}(t_m)]\xi_{\text{in}}(t) + \dots. \quad (\text{D24})$$

If we define the output state as

$$|\psi_{\text{out}}\rangle \equiv \int_{t_0}^{t_N} dt_m \int_{t_0}^{t_N} dt \xi_{\text{out}}(t_m, t) \hat{w}^\dagger(t_m) \hat{w}^\dagger(t) |\emptyset\rangle, \quad (\text{D25})$$

then the output wave packet is

$$\begin{aligned} \xi_{\text{out}}(t_m, t) &\equiv \xi_{\text{in}}(t_m)\xi_{\text{in}}(t) + \frac{1}{\sqrt{2}} \left[\sqrt{2\gamma}\psi_{20}(t_m)A_{10}(t_m, t) + \gamma\psi_{11}(t_m)B_{10}(t_m, t) - \sqrt{\gamma}\psi_{10}^{(2)}(t_m)\xi_{\text{in}}(t_m)A_{10}(t_m, t) \right. \\ &\quad \left. - \sqrt{\gamma}\psi_{01}^{(2)}(t_m)\xi_{\text{in}}(t_m)B_{10}(t_m, t) + \gamma\psi_{10}^{(2)}(t_m)\psi_{10}^{(1)}(t_m, t) - \sqrt{\gamma}\psi_{10}^{(2)}(t_m)\xi_{\text{in}}(t) - \sqrt{2\gamma}\xi_{\text{in}}(t_m)\psi_{10}^{(1)}(t_m, t) \right], \quad t_m \leq t, \end{aligned} \quad (\text{D26})$$

and $\xi_{\text{out}}(t_m, t) = \xi_{\text{out}}(t, t_m)$. The factor of $1/\sqrt{2}$ comes from the fact that the integrals in Eq. (D25) span the entire time interval, whereas the terms in Eqs. (D22)–(D24) were derived using the definition in Eq. (D1), where each two-photon field state appears only once in the summations.

The probability of finding the system in a state with n_a photons in mode a and n_b photons in mode b at time t_n is found from the expectation value

$$P_{n_a n_b}(t_n) = \langle \psi_n | (|n_a n_b\rangle \langle n_a n_b| \otimes \hat{\mathbb{I}}_{\text{field}}) | \psi_n \rangle = \sum_{j,k=1}^N |\langle 1_j 1_k | \langle n_a n_b | \psi_n \rangle|^2, \quad \text{with } \hat{\mathbb{I}}_{\text{field}} = \sum_{j,k=1}^N |1_j 1_k\rangle \langle 1_j 1_k|. \quad (\text{D27})$$

It is instructive to use Fig. 3 to keep track of all paths when evaluating the overlap $\langle 1_j 1_k | \langle n_a n_b | \psi_n \rangle$. For $n_a = n_b = 0$, we see that there are contributions from the two paths leading to states with one photon on the input side and one on the output side as well as contributions from both photons being on the input or output side. The first contribution may be identified from Eq. (D14)

$$\begin{aligned} |\langle 00|00\rangle|^2 &= \sum_{j',k'=1}^N \left| \sum_{m=1}^n \left([-\sqrt{\gamma} \psi_{10}^{(2)}(m) + \sqrt{2} \xi_m^{\text{in}}] \sum_{k>m} \xi_k^{\text{in}} \Delta t \langle 1_{j'} 1_{k'} | 1_k \mathbf{1}_m \rangle \right) \right|^2 \\ &= \sum_{k'=1}^n \sum_{j'=1}^N \left| [-\sqrt{\gamma} \psi_{10}^{(2)}(k') + \sqrt{2} \xi_{k'}^{\text{in}}] \sum_{k>k'} \xi_k^{\text{in}} \Delta t \langle 1_{j'} | 1_k \rangle \right|^2 = \sum_{k'=1}^n \Delta t \left| -\sqrt{\gamma} \psi_{10}^{(2)}(k') + \sqrt{2} \xi_{k'}^{\text{in}} \right|^2 \sum_{j'=k'}^N \Delta t |\xi_{j'}^{\text{in}}|^2, \end{aligned} \quad (\text{D28})$$

where the summation over m from 1 to n was included because the photon on the output side could be in any bin between 1 and n . The contribution from both photons being on the input side is

$$|\langle 00|00\rangle|^2 \sum_{j',k'=1}^N \sum_{m'>n} \Delta t |\xi_{m'}^{\text{in}}|^2 \sum_{m>n} \Delta t |\xi_m^{\text{in}}|^2 |\langle 1_{j'} 1_{k'} | 1_{m'} \mathbf{1}_m \rangle|^2 = \sum_{j'>n} \Delta t |\xi_{j'}^{\text{in}}|^2 \sum_{k'>n} \Delta t |\xi_{k'}^{\text{in}}|^2. \quad (\text{D29})$$

Similarly, the contribution from the output state is

$$|\langle 00|00\rangle|^2 \sum_{j',k'=1}^N \sum_{m'=1}^n \sum_{m=1}^n \Delta t \Delta t |\xi_{m'm}^{\text{out}}|^2 |\langle 1_{j'} 1_{k'} | \mathbf{1}_{m'} \mathbf{1}_m \rangle|^2 = \sum_{m'=1}^n \sum_{m=1}^n \Delta t \Delta t |\xi_{m'm}^{\text{out}}|^2. \quad (\text{D30})$$

Adding the contributions from Eqs. (D28)–(D30) and taking the continuum limit, we get

$$P_{00}(t_n) = \int_{t_0}^{t_n} \left(|\sqrt{2} \xi_{\text{in}}(t_m) - \gamma \psi_{10}^{(2)}(t_m)|^2 \int_{t_m}^{t_n} |\xi^{\text{in}}(s)|^2 ds \right) dt_m + \left(\int_{t_0}^{t_n} |\xi_{\text{in}}(t)|^2 dt \right)^2 + \int_{t_0}^{t_n} \int_{t_0}^{t_n} |\xi_{\text{out}}(t_m, s)|^2 ds dt_m. \quad (\text{D31})$$

There are seven different paths leading to the system state $|10\rangle$ and the probability is

$$\begin{aligned} P_{10}(t_n) &= |\psi_{10}^{(2)}(t_n)|^2 \int_{t_n}^{t_n} |\xi^{\text{in}}(s)|^2 ds + \int_{t_0}^{t_n} |\psi_{10}^{(2)}(t_m) \xi_{\text{in}}(t_m) A_{10}(t_m, t_n) + \psi_{01}^{(2)}(t_m) \xi_{\text{in}}(t_m) B_{10}(t_m, t_n) - \sqrt{2\gamma} \psi_{20}(t_m) A_{10}(t_m, t_n) \\ &\quad - \sqrt{\gamma} \psi_{11}(t_m) B_{10}(t_m, t_n) - \sqrt{\gamma} \psi_{10}^{(2)}(t_m) \psi_{10}^{(1)}(t_m, t_n) + \sqrt{2} \xi_{\text{in}}(t_m) \psi_{10}^{(1)}(t_m, t_n)|^2 dt_m. \end{aligned} \quad (\text{D32})$$

Similarly, the probability of the system state $|01\rangle$ is

$$\begin{aligned} P_{01}(t_n) &= |\psi_{01}^{(2)}(t_n)|^2 \int_{t_n}^{t_n} |\xi^{\text{in}}(s)|^2 ds + \int_{t_0}^{t_n} |\psi_{10}^{(2)}(t_m) \xi_{\text{in}}(t_m) A_{01}(t_m, t_n) + \psi_{01}^{(2)}(t_m) \xi_{\text{in}}(t_m) B_{01}(t_m, t_n) \\ &\quad - \sqrt{2\gamma} \psi_{20}(t_m) A_{01}(t_m, t_n) - \sqrt{\gamma} \psi_{11}(t_m) B_{01}(t_m, t_n) - \sqrt{\gamma} \psi_{10}^{(2)}(t_m) \psi_{01}^{(1)}(t_m, t_n) + \sqrt{2} \xi_{\text{in}}(t_m) \psi_{01}^{(1)}(t_m, t_n)|^2 dt_m. \end{aligned} \quad (\text{D33})$$

The probability distributions for states with two photons in the system are simply

$$P_{20}(t_n) = |\psi_{20}(t_n)|^2, \quad P_{11}(t_n) = |\psi_{11}(t_n)|^2, \quad P_{02}(t_n) = |\psi_{02}(t_n)|^2. \quad (\text{D34})$$

APPENDIX E: ABSORPTION OF PHOTON WAVEPACKET

We write the control function as $\Lambda(t) \equiv |\Lambda(t)| \exp[i\phi(t)]$ and our goal is to determine the amplitude, $|\Lambda(t)|$, and phase, $\phi(t)$, such that an incoming photon in the wave packet $\xi_{\text{in}}(t)$ is fully absorbed into mode b . The equations of motion are written in Eq. (C8), but we repeat them here for easy reference:

$$\dot{\psi}_{10}(t) = -\left[i\delta_a + \frac{\Gamma}{2} + i2|\Lambda(t)| \right] \psi_{10}(t) - i|\Lambda(t)| e^{-i\phi(t)} \psi_{01}(t) + \sqrt{\gamma} \xi(t), \quad (\text{E1a})$$

$$\dot{\psi}_{01}(t) = -\left[i\delta_b + \frac{\gamma L}{2} + i2|\Lambda(t)| \right] \psi_{01}(t) - i|\Lambda(t)| e^{i\phi(t)} \psi_{10}(t), \quad (\text{E1b})$$

$$\dot{\xi}_{\text{out}}(t) = \xi(t) - \sqrt{\gamma} \psi_{10}(t). \quad (\text{E1c})$$

Note that we have omitted the subscript of $\xi_{\text{in}}(t)$ in Eq. (E1) for notational convenience. Absorbing the incoming pulse implies $\xi_{\text{out}}=0$ and therefore $\psi_{10}=\xi_{\text{in}}/\sqrt{\gamma}$. Substituting this into Eq. (E1b) and rearranging terms yields

$$\frac{d}{dt}(\psi_{01}(t)e^{-Q(t)})e^{Q(t)} = \frac{-i}{\sqrt{\gamma}}|\Lambda(t)|e^{i\phi(t)}\xi(t) \Rightarrow \psi_{01}(t) = \frac{-i}{\sqrt{\gamma}}e^{Q(t)} \int_{t_0}^t e^{-Q(s)}|\Lambda(s)|e^{i\phi(s)}\xi(s)ds, \quad (\text{E2})$$

where we defined the functions

$$Q(t) = -iP(t) - \left(i\delta_b + \frac{\gamma_L}{2}\right)t, \quad P(t) = 2 \int_{t_0}^t |\Lambda(s)|ds. \quad (\text{E3})$$

Substituting $\psi_{10}=\xi/\sqrt{\gamma}$ into Eq. (E1a) yields

$$\frac{(\gamma - \gamma_L)}{2}\xi(t) - \dot{\xi}(t) - i[\delta_a + 2|\Lambda(t)|]\xi(t) = i|\Lambda(t)|e^{-i\phi(t)}\sqrt{\gamma}\psi_{01}(t). \quad (\text{E4})$$

Multiplying Eq. (E4) by $\xi(t)^*\exp(\gamma_L t)$ and defining real functions f_i and g_i , we find

$$f_i(t) + ig_i(t) = |\Lambda(t)|e^{-i\phi(t)}\xi(t)^*e^{(-i\delta_b + \frac{\gamma_L}{2})t}e^{-iP(t)} \int_{t_0}^t e^{(i\delta_b + \frac{\gamma_L}{2})s}e^{iP(s)}|\Lambda(s)|e^{i\phi(s)}\xi(s)ds, \quad (\text{E5})$$

with

$$f_i(t) = \left(\frac{\gamma - \gamma_L}{2}\xi(t) - \dot{\xi}(t)\right)\xi(t)^*e^{\gamma_L t}, \quad (\text{E6a})$$

$$g_i(t) = -(\delta_a + 2|\Lambda(t)|)|\xi(t)|^2e^{\gamma_L t}. \quad (\text{E6b})$$

Note that Eq. (E6a) assumes an input wave packet without chirp, $\frac{d}{dt}[\arg \xi(t)]=0$. The right-hand side (RHS) of Eq. (E5) can be written as

$$[x(t) - iy(t)] \int_{t_0}^t [x(s) + iy(s)]ds = x(t) \int_{t_0}^t x(s)ds + y(t) \int_{t_0}^t y(s)ds + i\left(x(t) \int_{t_0}^t y(s)ds - y(t) \int_{t_0}^t x(s)ds\right), \quad (\text{E7})$$

where

$$x(t) = |\Lambda(t)||\xi(t)| \exp(\gamma_L t/2) \cos[\phi(t) + \delta_b t + P(t) + \arg(\xi)], \quad (\text{E8a})$$

$$y(t) = |\Lambda(t)||\xi(t)| \exp(\gamma_L t/2) \sin[\phi(t) + \delta_b t + P(t) + \arg(\xi)]. \quad (\text{E8b})$$

By defining the functions

$$X(t) = \int_{t_0}^t x(s)ds = R(t) \cos[\theta(t)], \quad Y(t) = \int_{t_0}^t y(s)ds = R(t) \sin[\theta(t)], \quad (\text{E9})$$

Eq. (E5) can be split into real and imaginary parts

$$f_i = \dot{X}X + \dot{Y}Y, \quad g_i = \dot{X}Y - \dot{Y}X. \quad (\text{E10})$$

Using the definition in Eq. (E9), we have

$$f_i = \dot{X}X + \dot{Y}Y = [\dot{R} \cos(\theta) - R \sin(\theta)\dot{\theta}]R \cos(\theta) + [\dot{R} \sin(\theta) + R \cos(\theta)\dot{\theta}]R \sin(\theta) = \dot{R}R = \frac{1}{2} \frac{d}{dt}(R^2), \quad (\text{E11})$$

which has the solution

$$R(t) = \sqrt{2 \int_{t_0}^t f_i(s)ds}. \quad (\text{E12})$$

Similarly,

$$g_i = \dot{X}Y - \dot{Y}X = [\dot{R} \cos(\theta) - R \sin(\theta)\dot{\theta}]R \sin(\theta) - [\dot{R} \sin(\theta) + R \cos(\theta)\dot{\theta}]R \cos(\theta) = -R^2\dot{\theta}. \quad (\text{E13})$$

Using the result in Eq. (E12), the solution for θ is

$$\theta(t) = -\frac{1}{2} \int_{t_0}^t \frac{g_i(s)}{\int_{t_0}^s f_i(z)dz} ds. \quad (\text{E14})$$

To find the solution for $|\Lambda(t)|$, we evaluate $x^2 + y^2 = |\Lambda|^2|\xi|^2 \exp(\gamma_L t)$ using the results above

$$|\Lambda|^2|\xi|^2 e^{\gamma_L t} = \dot{X}^2 + \dot{Y}^2 = [\dot{R} \cos(\theta) - R \sin(\theta)\dot{\theta}]^2 + [\dot{R} \sin(\theta) + R \cos(\theta)\dot{\theta}]^2 = \dot{R}^2 + R^2\dot{\theta}^2 = \frac{1}{2 \int f_i} (g_i^2 + f_i^2). \quad (\text{E15})$$

Inserting the definition of g_i from Eq. (E6b) yields

$$\begin{aligned} |\Lambda|^2 |\xi|^2 \exp(\gamma_L t) &= \frac{1}{2\mathcal{F}_i} [(\delta_a + 2|\Lambda|)^2 \exp(2\gamma_L t) |\xi|^4 + f_i^2] \\ \Rightarrow |\Lambda(t)| &= \frac{2\delta_a |\xi|^4 e^{\gamma_L t} \pm \sqrt{2} e^{-\frac{\gamma_L}{2} t} |\xi| \sqrt{f_i^2 (\mathcal{F}_i - 2|\xi|^2 e^{\gamma_L t}) + \delta_a^2 |\xi|^4 \mathcal{F}_i e^{2\gamma_L t}}}{2|\xi|^2 [\mathcal{F}_i - 2|\xi|^2 e^{\gamma_L t}]}, \end{aligned} \quad (\text{E16})$$

where $\mathcal{F}_i(t)$ is the antiderivative of $f_i(t)$. If $\delta_a = 0$, the solution is

$$|\Lambda(t)| = \frac{|f_i(t)| e^{-\gamma_L t/2}}{\sqrt{2} |\xi(t)|} \frac{1}{\sqrt{\mathcal{F}_i - 2|\xi(t)|^2 e^{\gamma_L t}}}. \quad (\text{E17})$$

Knowing $|\Lambda(t)|$ means g_i is a known function and x and y may be evaluated using θ from Eq. (E14). Then, the phase ϕ is

$$\phi(t) = -\delta_b t - 2 \int_{t_0}^t |\Lambda(s)| ds - \arg(\xi) + \tan^{-1} \left[\frac{y(t)}{x(t)} \right]. \quad (\text{E18})$$

To obtain x and y , note that

$$x = \dot{X} = \dot{R} \cos(\theta) - R \sin(\theta) \dot{\theta} = \frac{f_i \cos(\theta) + g_i \sin(\theta)}{\sqrt{2 \int f_i}}, \quad (\text{E19})$$

$$y = \dot{Y} = \dot{R} \sin(\theta) + R \cos(\theta) \dot{\theta} = \frac{f_i \sin(\theta) - g_i \cos(\theta)}{\sqrt{2 \int f_i}}. \quad (\text{E20})$$

1. When does a solution exist?

From Eqs. (E6a) and (E16) it is seen that $|\Lambda(t)|$ is only a real finite function if (assuming ξ is real and there is no loss, $\gamma_L = 0$)

$$\begin{aligned} \int_{t_0}^t \left[\frac{\gamma}{2} \xi^2(s) ds - \xi(s) \dot{\xi}(s) \right] ds - 2\xi^2(t) &> 0 \\ \Rightarrow \frac{\gamma}{2} \int_{t_0}^t \xi^2(s) ds - \int_{t_0}^t \frac{1}{2} \frac{d}{ds} [\xi^2(s)] ds - 2\xi^2(t) &> 0 \quad \Rightarrow \quad \xi^2(t) < \frac{\gamma}{5} \int_{t_0}^t \xi^2(s) ds. \end{aligned} \quad (\text{E21})$$

A general identity holds for inequalities of the type in Eq. (E21) [48]

$$\dot{u}(t) \leq \beta(t) u(t) \Rightarrow u(t) \leq u(a) \exp \left(\int_a^t \beta(s) ds \right). \quad (\text{E22})$$

Comparing Eq. (E22) to Eq. (E21) shows that

$$u(t) \leq u(0) \exp \left(\frac{\gamma}{5} t \right), \quad u(t) \equiv \int_{t_0}^t \xi^2(s) ds. \quad (\text{E23})$$

Since $u(0)$ should equal zero, we see that this cannot be fulfilled. If $t=0$ is excluded from the interval over which the solution must be valid, then $u(0^+)$ can be made arbitrarily small and Eq. (E23) provides a bound on what the rising edge of the wave packet can look like. However, since $u(T) = 1$ in order for the input quantum state to be normalized, we see that the wave-packet length increases as $u(0^+)$ decreases. In physical terms, a finite-length wave packet cannot be fully absorbed into a resonator without letting the coupling rate, γ , tend to infinity, if only for an infinitely short time. This is because the exponential decay out of the resonator only asymptotically approaches a state where the entire cavity population has coupled into the waveguide.

We note that if there is no cross-phase modulation from the control fields, the decay rate $\gamma/5$ in Eq. (E23) would instead be γ , suggesting that the same absorption efficiency could be achieved with a cavity mode having a linewidth five times smaller.

APPENDIX F: EMISSION OF PHOTON WAVE PACKET

The goal of this section is to derive a control field, Λ , such that the output wave packet, ξ_{out} , is given by some desired function, ξ . In this case, the driving term, $\xi_{\text{in}} = 0$, and the initial condition is that $\psi_{10}(0) = 0$ while the Schrödinger coefficient corresponding to state $|01\rangle$ has some finite value, $\psi_{01}(0)$. The equations of motion are

$$\dot{\psi}_{10}(t) = - \left[i\delta_a + \frac{\Gamma}{2} + i2|\Lambda(t)| \right] \psi_{10}(t) - i|\Lambda(t)| e^{-i\phi(t)} \psi_{01}(t), \quad (\text{F1a})$$

$$\dot{\psi}_{01}(t) = - \left[i\delta_b + \frac{\gamma_L}{2} + i2|\Lambda(t)| \right] \psi_{01}(t) - i|\Lambda(t)| e^{i\phi(t)} \psi_{10}(t), \quad (\text{F1b})$$

$$\dot{\xi}(t) = -\sqrt{\gamma} \psi_{10}(t). \quad (\text{F1c})$$

Substituting $\psi_{10} = -\xi/\sqrt{\gamma}$ into Eq. (F1), we have

$$\dot{\xi} = -\left(\frac{\Gamma}{2} + i(\delta_a + 2|\Lambda|)\right)\xi + i|\Lambda|e^{-i\phi}\sqrt{\gamma}\psi_{01}, \quad (\text{F2})$$

$$\dot{\psi}_{01}(t) = -\left(i\delta_b + \frac{\gamma_L}{2} + i2|\Lambda|\right)\psi_{01} + i\frac{|\Lambda|e^{i\phi}}{\sqrt{\gamma}}\xi. \quad (\text{F3})$$

Using the same functions $P(t)$ and $Q(t)$ as in Appendix E, Eq. (F3) can be solved:

$$\begin{aligned} \frac{d}{dt}(\psi_{01}(t)e^{-Q(t)})e^{Q(t)} &= i\frac{|\Lambda(t)|e^{i\phi(t)}}{\sqrt{\gamma}}\xi(t) \Rightarrow \psi_{01}(t)e^{-Q(t)} - \psi_{01}(0) = \frac{i}{\sqrt{\gamma}}\int_{t_0}^t |\Lambda(s)|e^{i\phi(s)}\xi(s)e^{-Q(s)}ds \\ \Rightarrow \psi_{01}(t) &= e^{Q(t)}\left[\psi_{01}(0) + \frac{i}{\sqrt{\gamma}}\int_{t_0}^t |\Lambda(s)|e^{i\phi(s)}\xi(s)e^{-Q(s)}ds\right]. \end{aligned} \quad (\text{F4})$$

Comparing Eqs. (F4) and (F2), we see that

$$\dot{\xi}(t) + \frac{\Gamma}{2}\xi(t) + i(\delta_a + 2|\Lambda(t)|)\xi(t) = i|\Lambda(t)|e^{-i\phi(t)}\sqrt{\gamma}e^{Q(t)}\left[\psi_{01}(0) + \frac{i}{\sqrt{\gamma}}\int_{t_0}^t |\Lambda(s)|e^{i\phi(s)}\xi(s)e^{-Q(s)}ds\right]. \quad (\text{F5})$$

Multiplying both sides by $-\xi^* \exp[\gamma_L t]$ yields

$$\begin{aligned} -\left(\dot{\xi}(t) + \frac{\Gamma}{2}\xi(t)\right)\xi(t)^* e^{\gamma_L t} - i(\delta_a + 2|\Lambda(t)|)|\xi(t)|^2 e^{\gamma_L t} \\ = -i|\Lambda(t)|e^{-i\phi(t)}\xi(t)^* e^{(-i\delta_b + \frac{\gamma_L}{2})t} e^{-iP(t)}\left[\psi_{01}(0)\sqrt{\gamma} + \int_{t_0}^t i|\Lambda(s)|e^{i\phi(s)}\xi(s)e^{(i\delta_b + \frac{\gamma_L}{2})s} e^{iP(s)}ds\right]. \end{aligned} \quad (\text{F6})$$

Let us assume that $\psi_{01}(0)$ is complex valued with a phase θ_0 . Then, Eq. (F6) can be rewritten as (where LHS denotes left-hand side)

$$\begin{aligned} \text{LHS} &= -i|\Lambda(t)|e^{-i\phi(t)}\xi(t)^* e^{(-i\delta_b + \frac{\gamma_L}{2})t} e^{-iP(t)}\left[|\psi_{01}(0)|e^{i\theta_0}\sqrt{\gamma} + \int_{t_0}^t i|\Lambda(s)|e^{i\phi(s)}\xi(s)e^{(i\delta_b + \frac{\gamma_L}{2})s} e^{iP(s)}ds\right], \\ \text{LHS} \times e^{-i\theta_0} &= -i|\Lambda(t)|e^{-i\phi(t)}\xi(t)^* e^{(-i\delta_b + \frac{\gamma_L}{2})t} e^{-iP(t)}\left[|\psi_{01}(0)|\sqrt{\gamma} + \int_{t_0}^t i|\Lambda(s)|e^{i\phi(s)}(\xi(s)e^{-i\theta_0})e^{(i\delta_b + \frac{\gamma_L}{2})s} e^{iP(s)}ds\right], \\ \text{LHS} &= -i|\Lambda(t)|e^{-i\phi(t)}(\xi(t)^* e^{i\theta_0})e^{(-i\delta_b + \frac{\gamma_L}{2})t} e^{-iP(t)}\left[|\psi_{01}(0)|\sqrt{\gamma} + \int_{t_0}^t i|\Lambda(s)|e^{i\phi(s)}(\xi(s)e^{-i\theta_0})e^{(i\delta_b + \frac{\gamma_L}{2})s} e^{iP(s)}ds\right]. \end{aligned} \quad (\text{F7})$$

Equation (F7) may be written as

$$-f_o + ig_o = (x - iy)\left(C + \int_{t_0}^t [x(s) + iy(s)]ds\right) = x\left[C + \int_{t_0}^t x(s)ds\right] + y\int_{t_0}^t y(s)ds + i\left(x\int_{t_0}^t y(s)ds - y\left[C + \int_{t_0}^t x(s)ds\right]\right), \quad (\text{F8})$$

where

$$C = |\psi_{01}(0)|\sqrt{\gamma}, \quad (\text{F9a})$$

$$x = -|\Lambda(t)||\xi(t)|\exp(\gamma_L t/2)\sin[\phi(t) + \delta_b t + P(t) + \arg(\xi) - \theta_0], \quad (\text{F9b})$$

$$y = |\Lambda(t)||\xi(t)|\exp(\gamma_L t/2)\cos[\phi(t) + \delta_b t + P(t) + \arg(\xi) - \theta_0], \quad (\text{F9c})$$

$$f_o = \left(\dot{\xi}(t) + \frac{\Gamma}{2}\xi(t)\right)\xi(t)^* e^{\gamma_L t}, \quad (\text{F9d})$$

$$g_o = -(\delta_a + 2|\Lambda(t)|)|\xi(t)|^2 e^{\gamma_L t}. \quad (\text{F9e})$$

Let us define the functions

$$X(t) = C + \int_{t_0}^t x(s)ds = R(t)\cos[\theta(t)], \quad Y(t) = \int_{t_0}^t y(s)ds = R(t)\sin[\theta(t)]. \quad (\text{F10})$$

Equating real and imaginary parts of Eq. (F8) yields

$$-f_o(t) = \dot{X}(t)X(t) + \dot{Y}(t)Y(t), \quad g_o(t) = \dot{X}(t)Y(t) - \dot{Y}(t)X(t), \quad (\text{F11})$$

where $x(t)=\dot{X}(t)$ and $y(t)=\dot{Y}(t)$. Using the definition in Eq. (F10), we have

$$\begin{aligned} -f_o &= \dot{X}X + \dot{Y}Y = [\dot{R}\cos(\theta) - R\sin(\theta)\dot{\theta}]R\cos(\theta) + [\dot{R}\sin(\theta) + R\cos(\theta)\dot{\theta}]R\sin(\theta) = \dot{R}R = \frac{1}{2}\frac{d}{dt}(R^2) \\ \Rightarrow R(t)^2 - R(0)^2 &= -\int_{t_0}^t 2f_o(s)ds. \end{aligned} \quad (\text{F12})$$

Since $R^2 = X^2 + Y^2$, we have $R(0)^2 = C^2$ and therefore

$$R(t) = \sqrt{C^2 - 2\int_{t_0}^t f_o(s)ds}. \quad (\text{F13})$$

Similarly,

$$g_o = \dot{X}Y - \dot{Y}X = [\dot{R}\cos(\theta) - R\sin(\theta)\dot{\theta}]R\sin(\theta) - [\dot{R}\sin(\theta) + R\cos(\theta)\dot{\theta}]R\cos(\theta) = -R^2\dot{\theta}. \quad (\text{F14})$$

Using the result in Eq. (F13) and the initial condition $\theta(0)=0$, the solution for θ is

$$\theta(t) = -\int_{t_0}^t \frac{g_o(s)}{C^2 - 2\int_{t_0}^s f_o(z)dz} ds. \quad (\text{F15})$$

To find the solution for $|\Lambda(t)|$, we evaluate $x^2 + y^2 = |\Lambda|^2|\xi|^2 \exp(\gamma_L t)$ using the results above

$$|\Lambda|^2|\xi|^2 e^{\gamma_L t} = \dot{X}^2 + \dot{Y}^2 = [\dot{R}\cos(\theta) - R\sin(\theta)\dot{\theta}]^2 + [\dot{R}\sin(\theta) + R\cos(\theta)\dot{\theta}]^2 = \dot{R}^2 + R^2\dot{\theta}^2 = \frac{g_o^2 + f_o^2}{C^2 - 2\int f_o}. \quad (\text{F16})$$

Inserting the definition of g_o from Eq. (F9e) yields

$$\begin{aligned} |\Lambda|^2|\xi|^2 \exp(\gamma_L t) &= \frac{1}{C^2 - 2\mathcal{F}_o} [(\delta_a + 2|\Lambda|)^2 \exp(2\gamma_L t)|\xi|^4 + f_o^2] \\ \Rightarrow |\Lambda(t)| &= e^{-\gamma_L t} \frac{2\delta_a|\xi|^3 e^{2\gamma_L t} \pm \sqrt{e^{\gamma_L t} f_o^2 (C^2 - 2\mathcal{F}_o - 4e^{2\gamma_L t} \xi^2) + \delta_a^2 \xi^4 (C^2 - 2\mathcal{F}_o) e^{3\gamma_L t}}}{|\xi| [C^2 - 2\mathcal{F}_o - 4\xi^2 e^{\gamma_L t}]}, \end{aligned} \quad (\text{F17})$$

where $\mathcal{F}_o(t)$ is the antiderivative of $f_o(t)$. If $\delta_a=0$, the solution is

$$|\Lambda(t)| = \frac{|f_o| \exp(-\gamma_L t/2)}{|\xi|} \frac{1}{\sqrt{C^2 - 2\mathcal{F}_o - 4|\xi|^2 e^{\gamma_L t}}}. \quad (\text{F18})$$

Knowing $|\Lambda(t)|$ means g_o is a known function and x and y may be evaluated using θ from Eq. (F15). Then, the phase ϕ is

$$\phi(t) = -\delta_b t - 2 \int_{t_0}^t |\Lambda(s)| ds - \arg(\xi) + \theta_0 + \tan^{-1} \left[\frac{-x(t)}{y(t)} \right]. \quad (\text{F19})$$

To obtain x and y , note that

$$x = \dot{X} = \dot{R}\cos(\theta) - R\sin(\theta)\dot{\theta} = \frac{-f_o \cos(\theta) + g_o \sin(\theta)}{\sqrt{C^2 - 2\int f_o}}, \quad (\text{F20})$$

$$y = \dot{Y} = \dot{R}\sin(\theta) + R\cos(\theta)\dot{\theta} = \frac{-f_o \sin(\theta) - g_o \cos(\theta)}{\sqrt{C^2 - 2\int f_o}}. \quad (\text{F21})$$

1. Gaussian Wave Packet

The Gaussian wave packet is

$$\xi_{\text{in}}(t) = \mathcal{G}(t - T_i) = \sqrt{\frac{2}{\tau_g}} \left(\frac{\ln(2)}{\pi} \right)^{\frac{1}{4}} \exp \left[-2\ln(2) \frac{(t - T_i)^2}{\tau_g^2} \right], \quad (\text{F22})$$

where $|\mathcal{G}(t)|^2$ has a full width at half maximum (FWHM) temporal width τ_g and spectral width $\Omega_g = 4\ln(2)/\tau_g$, and integrates to 1 (over the infinite interval from $-\infty$ to ∞). As discussed in Appendix E 1, it is not possible to fully absorb this wave packet and this issue manifests in the denominator of Eq. (E16) being imaginary during the rising edge of the Gaussian where

$$2 \int_{t_0}^t f_i(s) ds - 4|\xi_{\text{in}}(t)|^2 e^{\gamma_L t} \leq 0. \quad (\text{F23})$$

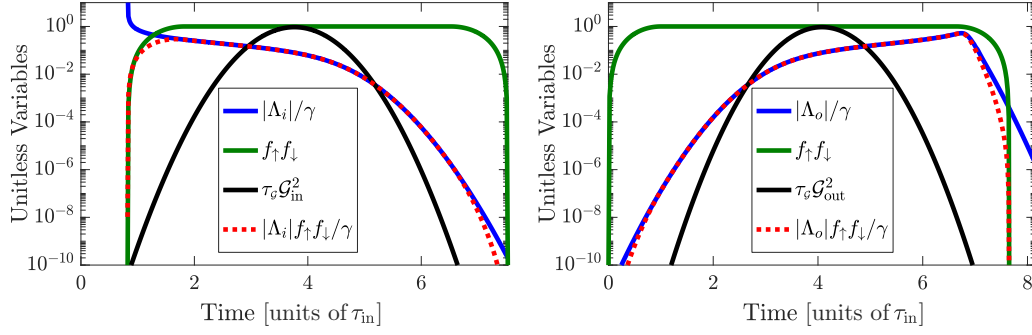


FIG. 10. Illustration of the solutions for $|\Lambda_{i/o}|$ along with the smoothing functions in Eq. (F24) that ensures well-behaved control fields. Parameters: (a) $\gamma = 30\Omega_G$, $\gamma_L = 0$, $\tau_e = \tau_G$. (b) $\gamma_L = 10^{-5}\Omega_G$.

$|\Lambda|$ diverges at the cross point determined by an equality in Eq. (F23). This is illustrated in Fig. 10 (blue curve). To avoid divergences and keep $|\Lambda|$ real, we multiply the solution in Eq. (E16) by smoothing functions

$$f_{\uparrow}(t) = \frac{1 + \sin\left(\frac{\pi t}{\tau_e}\right)}{2} \Theta\left(t + \frac{\tau_e}{2}\right) \Theta\left(\frac{\tau_e}{2} - t\right) + \Theta\left(t - \frac{\tau_e}{2}\right), \quad (\text{F24})$$

$$f_{\downarrow}(t) = \frac{1 - \sin\left(\frac{\pi t}{\tau_e}\right)}{2} \Theta\left(t + \frac{\tau_e}{2}\right) \Theta\left(\frac{\tau_e}{2} - t\right) + \Theta\left(-\frac{\tau_e}{2} - t\right), \quad (\text{F25})$$

where Θ is a step function that equals 1 for positive arguments and 0 for negative arguments. The smoothing functions rise from 0 to 1 (f_{\uparrow}) or fall from 1 to 0 (f_{\downarrow}) in the interval $t \in [-\tau_e/2, \tau_e/2]$ as half a period of the sine function.

APPENDIX G: INPUT PUMP FIELDS FOR ABSORPTION AND EMISSION

The resonator modes that couple to the pump fields are identical and the Hamiltonian associated with those modes is

$$\hat{H}_n^{\text{pump}} = i\hbar \sqrt{\frac{\gamma_p}{\Delta t}} \sum_{m=1}^2 (\hat{p}_m^\dagger \hat{W}_n - \hat{p}_m \hat{W}_n^\dagger) + \hbar \chi_3 \hat{p}_1^\dagger \hat{p}_1 \hat{p}_2^\dagger \hat{p}_2 + \frac{1}{4} \hbar \chi_3 \sum_{m=1}^2 (\hat{p}_m^\dagger \hat{p}_m - 1) \hat{p}_m^\dagger \hat{p}_m. \quad (\text{G1})$$

The temporal shape of the input pump functions can be found by considering their equations of motion

$$\dot{\alpha}_1 = \left(-\frac{\Gamma_p}{2} - i\chi_3 \left[\frac{|\alpha_1|^2}{2} + |\alpha_2|^2\right]\right) \alpha_1 + \sqrt{\gamma_p} \xi_1, \quad (\text{G2a})$$

$$\dot{\alpha}_2 = \left(-\frac{\Gamma_p}{2} - i\chi_3 \left[|\alpha_1|^2 + \frac{|\alpha_2|^2}{2}\right]\right) \alpha_2 + \sqrt{\gamma_p} \xi_2. \quad (\text{G2b})$$

In Sec. III, we assumed that $|\alpha_1| = |\alpha_2|$, so we can write $\Lambda = \chi_3 \alpha_2^* \alpha_1 = |\Lambda| \exp(i\phi) = \chi_3 r_\alpha^2 \exp[i(\phi_1 - \phi_2)]$, where $\alpha_1 = r_\alpha \exp(i\phi_1)$ and $\alpha_2 = r_\alpha \exp(i\phi_2)$ with $\phi = \phi_1 - \phi_2$. The goal is to determine the complex-valued input fields, ξ_1 and ξ_2 , such that Eq. (G2) yields the correct intracavity control fields α_1 and α_2 . Let us write the pump fields in polar form: $\xi_n = q_n \exp(i\psi_n)$ and substitute into Eq. (G2)

$$\dot{\alpha}_n = (\dot{r}_\alpha + i\dot{\phi}_n r_\alpha) e^{i\phi_n} = \left(-\frac{\Gamma_p}{2} - i\frac{3}{2} \chi_3 r_\alpha^2\right) r_\alpha e^{i\phi_n} + \sqrt{\gamma_p} q_n e^{i\psi_n}. \quad (\text{G3})$$

Separating equations for the real and imaginary parts yields

$$\dot{r}_\alpha = -\frac{\Gamma_p}{2} r_\alpha + \sqrt{\gamma_p} q_n \cos(\psi_n - \phi_n), \quad (\text{G4a})$$

$$\dot{\phi}_n = -\frac{3}{2} \chi_3 r_\alpha^2 + \sqrt{\gamma_p} \frac{q_n}{r_\alpha} \sin(\psi_n - \phi_n). \quad (\text{G4b})$$

Let us guess that $q_1 = q_2 = q$ and $\psi_1 - \phi_1 = -(\psi_2 - \phi_2)$. Since $\phi = \phi_1 - \phi_2$, we have

$$\dot{\phi} = \dot{\phi}_1 - \dot{\phi}_2 = \sqrt{\gamma_p} \frac{q}{r_\alpha} [\sin(\psi_1 - \phi_1) - \sin(\psi_2 - \phi_2)] = 2\sqrt{\gamma_p} \frac{q}{r_\alpha} \sin(\psi_1 - \phi_1). \quad (\text{G5})$$

Rearranging Eqs. (G4a) and (G5), we have

$$\frac{1}{2} \frac{r_\alpha \dot{\phi}}{\left(\dot{r}_\alpha + \frac{\Gamma_p}{2} r_\alpha\right)} = \tan(\psi_1 - \phi_1), \Rightarrow \psi_1 - \phi_1 = \arctan \left[\frac{1}{2} \frac{r_\alpha \dot{\phi}}{\left(\dot{r}_\alpha + \frac{\Gamma_p}{2} r_\alpha\right)} \right]. \quad (\text{G6})$$

Using the identity $\cos[\arctan(x)] = 1/\sqrt{1+x^2}$, we find q from Eq. (G4a)

$$\dot{i}_\alpha + \frac{\Gamma_p}{2} r_\alpha = \sqrt{\gamma_p} q \frac{1}{\sqrt{1 + \frac{1}{4} \left(\frac{r_\alpha \dot{\phi}}{\dot{i}_\alpha + \frac{\Gamma_p}{2} r_\alpha} \right)^2}}, \Rightarrow q = \frac{1}{\sqrt{\gamma_p}} \sqrt{\left(\dot{i}_\alpha + \frac{\Gamma_p}{2} r_\alpha \right)^2 + \frac{\dot{\phi}^2 r_\alpha^2}{4}}. \quad (\text{G7})$$

Using the identity $\sin[\arctan(x)] = x/\sqrt{1+x^2}$, we may insert Eq. (G6) into Eq. (G4b) to obtain

$$\dot{\phi}_1 = -\frac{3}{2} \chi_3 r_\alpha^2 + \sqrt{\gamma_p} \frac{q}{r_\alpha} \left[\frac{1}{2} \frac{r_\alpha \dot{\phi}}{\left(\dot{i}_\alpha + \frac{\Gamma_p}{2} r_\alpha \right)} \right] \frac{1}{\sqrt{1 + \frac{1}{4} \left(\frac{r_\alpha \dot{\phi}}{\dot{i}_\alpha + \frac{\Gamma_p}{2} r_\alpha} \right)^2}} = -\frac{3}{2} \chi_3 r_\alpha^2 + \frac{\dot{\phi}}{2}, \quad (\text{G8a})$$

$$\dot{\phi}_2 = -\frac{3}{2} \chi_3 r_\alpha^2 - \frac{\dot{\phi}}{2}. \quad (\text{G8b})$$

Integrating Eq. (G8), and inserting into Eq. (G6), we find

$$\psi_1(t) = -\frac{3}{2} \int_0^t |\Lambda(s)| ds + \frac{\phi(t)}{2} + \arctan \left[\frac{1}{2} \frac{r_\alpha \dot{\phi}}{\left(\dot{i}_\alpha + \frac{\Gamma_p}{2} r_\alpha \right)} \right], \quad (\text{G9a})$$

$$\psi_2(t) = -\frac{3}{2} \int_0^t |\Lambda(s)| ds - \frac{\phi(t)}{2} - \arctan \left[\frac{1}{2} \frac{r_\alpha \dot{\phi}}{\left(\dot{i}_\alpha + \frac{\Gamma_p}{2} r_\alpha \right)} \right]. \quad (\text{G9b})$$

-
- [1] H. J. Kimble, The quantum internet, *Nature (London)* **453**, 1023 (2008).
- [2] S. Hu and S. M. Weiss, Design of photonic crystal cavities for extreme light concentration, *ACS Photon.* **3**, 1647 (2016).
- [3] H. Choi, M. Heuck, and D. Englund, Self-Similar Nanocavity Design with Ultrasmall Mode Volume for Single-Photon Non-linearities, *Phys. Rev. Lett.* **118**, 223605 (2017).
- [4] S. Hu, M. Khater, R. Salas-Montiel, E. Kratschmer, S. Engelmann, W. M. J. Green, and S. M. Weiss, Experimental realization of deep subwavelength confinement in dielectric optical resonators, *Sci. Adv.* **4**, eaat2355 (2018).
- [5] M. Zhang, C. Wang, Y. Hu, A. Shams-Ansari, T. Ren, S. Fan, and M. Lončar, Electronically programmable photonic molecule, *Nat. Photon.* **13**, 36 (2019).
- [6] H. Liang, R. Luo, Y. He, H. Jiang, and Q. Lin, High-quality lithium niobate photonic crystal nanocavities, *Optica* **4**, 1251 (2017).
- [7] G. Lenz, B. J. Eggleton, C. K. Madsen, and R. E. Slusher, Optical delay lines based on optical filters, *IEEE J. Quantum Electron.* **37**, 525 (2001).
- [8] Y. Tanaka, J. Upham, T. Nagashima, T. Sugiya, T. Asano, and S. Noda, Dynamic control of the Q factor in a photonic crystal nanocavity, *Nat. Mater.* **6**, 862 (2007).
- [9] Q. Xu, P. Dong, and M. Lipson, Breaking the delay-bandwidth limit in a photonic structure, *Nat. Phys.* **3**, 406 (2007).
- [10] C. J. McKinstrie, J. D. Harvey, S. Radic, and M. G. Raymer, Translation of quantum states by four-wave mixing in fibers, *Opt. Express* **13**, 9131 (2005).
- [11] Q. Li, M. Davanco, and K. Srinivasan, Efficient and low-noise single-photon-level frequency conversion interfaces using silicon nanophotonics, *Nat. Photon.* **10**, 406 (2016).
- [12] M. Heuck, J. G. Koefoed, J. B. Christensen, Y. Ding, L. H. Frandsen, K. Rottwitz, and L. K. Oxenlowe, Unidirectional frequency conversion in microring resonators for on-chip frequency-multiplexed single-photon sources, *New J. Phys.* **21**, 033037 (2019).
- [13] X. Guo, C.-L. Zou, H. Jung, and H. X. Tang, On-Chip Strong Coupling and Efficient Frequency Conversion Between Telecom and Visible Optical Modes, *Phys. Rev. Lett.* **117**, 123902 (2016).
- [14] C. K. Madsen, G. Lenz, A. J. Bruce, M. A. Cappuzzo, L. T. Gomez, and R. E. Scotti, Integrated all-pass filters for tunable dispersion and dispersion slope compensation, *IEEE Photon. Technol. Lett.* **11**, 1623 (1999).
- [15] D. V. Reddy and M. G. Raymer, Photonic temporal-mode multiplexing by quantum frequency conversion in a dichroic-finesse cavity, *Opt. Express* **26**, 28091 (2018).
- [16] M. J. Collett and C. W. Gardiner, Squeezing of intracavity and traveling-wave light fields produced in parametric amplification, *Phys. Rev. A* **30**, 1386 (1984).
- [17] C. W. Gardiner and M. J. Collett, Input and output in damped quantum systems: Quantum stochastic differential equations and the master equation, *Phys. Rev. A* **31**, 3761 (1985).
- [18] R. Cook, D. I. Schuster, A. N. Cleland, and K. Jacobs, Input-output theory for superconducting and photonic circuits that contain weak retroreflections and other weak pseudocavities, *Phys. Rev. A* **98**, 013801 (2018).
- [19] K. Kojima, H. F. Hofmann, S. Takeuchi, and K. Sasaki, Non-linear interaction of two photons with a one-dimensional atom: Spatiotemporal quantum coherence in the emitted field, *Phys. Rev. A* **68**, 013803 (2003).
- [20] J.-T. Shen and S. Fan, Strongly correlated multiparticle transport in one dimension through a quantum impurity, *Phys. Rev. A* **76**, 062709 (2007).
- [21] J.-T. Shen and S. Fan, Strongly Correlated Two-Photon Transport in a One-Dimensional Waveguide Coupled to a Two-Level System, *Phys. Rev. Lett.* **98**, 153003 (2007).

- [22] T. Shi and C. P. Sun, Lehmann-Symanzik-Zimmermann reduction approach to multiphoton scattering in coupled-resonator arrays, *Phys. Rev. B* **79**, 205111 (2009).
- [23] S. Fan, S. E. Kocabaş, and J.-T. Shen, Input-output formalism for few-photon transport in one-dimensional nanophotonic waveguides coupled to a qubit, *Phys. Rev. A* **82**, 063821 (2010).
- [24] T. Shi, S. Fan, and C. P. Sun, Two-photon transport in a waveguide coupled to a cavity in a two-level system, *Phys. Rev. A* **84**, 063803 (2011).
- [25] D. Valente, Y. Li, J. P. Poizat, J. M. Gérard, L. C. Kwek, M. F. Santos, and A. Auffèves, Optimal irreversible stimulated emission, *New J. Phys.* **14**, 083029 (2012).
- [26] S. Xu and S. Fan, Input-output formalism for few-photon transport: A systematic treatment beyond two photons, *Phys. Rev. A* **91**, 043845 (2015).
- [27] Y. Pan, D. Dong, and G. Zhang, Exact analysis of the response of quantum systems to two-photons using a QSDE approach, *New J. Phys.* **18**, 033004 (2016).
- [28] M. P. Schneider, T. Sproll, C. Stawiarski, P. Schmitteckert, and K. Busch, Green's-function formalism for waveguide QED applications, *Phys. Rev. A* **93**, 013828 (2016).
- [29] S. Xu and S. Fan, Generalized cluster decomposition principle illustrated in waveguide quantum electrodynamics, *Phys. Rev. A* **95**, 063809 (2017).
- [30] P. Longo, P. Schmitteckert, and K. Busch, Dynamics of photon transport through quantum impurities in dispersion-engineered one-dimensional systems, *J. Opt. A: Pure Appl. Opt.* **11**, 114009 (2009).
- [31] P. Longo, P. Schmitteckert, and K. Busch, Few-Photon Transport in Low-Dimensional Systems: Interaction-Induced Radiation Trapping, *Phys. Rev. Lett.* **104**, 023602 (2010).
- [32] A. Nysteen, P. T. Kristensen, D. P. S. McCutcheon, P. Kaer, and J. Mørk, Scattering of two photons on a quantum emitter in a one-dimensional waveguide: Exact dynamics and induced correlations, *New J. Phys.* **17**, 023030 (2015).
- [33] T. Caneva, M. T. Manzoni, T. Shi, J. S. Douglas, J. I. Cirac, and D. E. Chang, Quantum dynamics of propagating photons with strong interactions: A generalized input-output formalism, *New J. Phys.* **17**, 113001 (2015).
- [34] R. Trivedi, K. Fischer, S. Xu, S. Fan, and J. Vuckovic, Few-photon scattering and emission from low-dimensional quantum systems, *Phys. Rev. B* **98**, 144112 (2018).
- [35] B. Q. Baragiola, R. L. Cook, A. M. Brańczyk, and J. Combes, N-photon wave packets interacting with an arbitrary quantum system, *Phys. Rev. A* **86**, 013811 (2012).
- [36] V. Scarani, M. Ziman, P. Štelmachovič, N. Gisin, and V. Bužek, Thermalizing Quantum Machines: Dissipation and Entanglement, *Phys. Rev. Lett.* **88**, 097905 (2002).
- [37] F. Ciccarello, Collision models in quantum optics, *Quantum Meas. Quantum Metrol.* **4**, 53 (2017).
- [38] J. A. Gross, C. M. Caves, G. J. Milburn, and J. Combes, Qubit models of weak continuous measurements: Markovian conditional and open-system dynamics, *Quantum Sci. Technol.* **3**, 024005 (2018).
- [39] Z. Vernon, M. Liscidini, and J. E. Sipe, Quantum frequency conversion and strong coupling of photonic modes using four-wave mixing in integrated microresonators, *Phys. Rev. A* **94**, 023810 (2016).
- [40] H. A. Haus, *Waves and Fields in Optoelectronics*, 1st ed. (Prentice-Hall, Englewood Cliffs, NJ, 1984).
- [41] K. Jacobs, *Quantum Measurement Theory and Its Applications* (Cambridge University Press, Cambridge, UK, 2014).
- [42] P. Kok and B. W. Lovett, *Optical Quantum Information Processing*, 1st ed. (Cambridge University Press, Cambridge, UK, 2010).
- [43] E. Knill, G. Milburn, and R. Laflamme, A scheme for efficient quantum computation with linear optics, *Nature (London)* **409**, 46 (2001).
- [44] A. Nysteen, D. P. S. McCutcheon, M. Heuck, J. Mørk, and D. R. Englund, Limitations of two-level emitters as nonlinearities in two-photon controlled-PHASE gates, *Phys. Rev. A* **95**, 062304 (2017).
- [45] M. Heuck, K. Jacobs, and D. R. Englund, Controlled-Phase Gate Using Dynamically Coupled Cavities and Optical Nonlinearities, *Phys. Rev. Lett.* **124**, 160501 (2020).
- [46] E. Timurdogan, C. V. Poulton, M. J. Byrd, and M. R. Watts, Electric field-induced second-order nonlinear optical effects in silicon waveguides, *Nat. Photon.* **11**, 200 (2017).
- [47] J. I. Cirac, P. Zoller, H. J. Kimble, and H. Mabuchi, Quantum State Transfer and Entanglement Distribution among Distant Nodes in a Quantum Network, *Phys. Rev. Lett.* **78**, 3221 (1997).
- [48] T. H. Gronwall, Note on the derivatives with respect to a parameter of the solutions of a system of differential equations, *Ann. Math.* **20**, 292 (1919).